Politechnika Warszawska

W Y D Z I A Ł   F I Z Y K I

Praca dyplomowa magisterska

na kierunku Fizyka Techniczna
w specjalności Fizyka i Technika Jądrowa

Optimalisation of track reconstruction using vertex detector in the NA61/SHINE experiment

Wojciech Bryliński

Numer albumu 261553

opiekun
dr inż. Dariusz Tefelski
opiekun zewnętrzny
dr hab. Paweł Staszel

WARSZAWA 2018

Acknowledgements

I would like to express enormous gratitude to my Supervisors: Dariusz Tefelski and Paweł Staszel, for the constant support and for guiding me through the whole analysis. Thanks to you, I really enjoyed working on this thesis. Thank you!

I also wish to thank very much all the people from the NA61/SHINE Collaboration. I had many opportunities to spend a wonderful time in the experiment, meeting very interesting scientists and having many discussions – not only about physics.

I am thankful to the NA61/SHINE group at the Faculty of Physics, Warsaw University of Technology, especially to Katarzyna Grebieszkow for creating warm and family atmosphere in the group. Special thanks to the NA61/SHINE DCS group: Tobiasz Czopowicz and Bartosz Maksiak (thanks to you I joined the NA61/SHINE experiment!). It is a fantastic experience to have even a small input to the Detector Control System.

Finally, I would like to express my gratitude to all my friends which I met during the studies; Rafał, Monika, Justyna, Ewa, Maciek and many others. With many of you I spent a great time while being at CERN.

Last but not least, I would like to thank my family; my parents and my brothers: Piotr, Krzysztof and Łukasz. Especially, I wish to thank my brother and best friend – Paweł Bryliński with whom I was living for three years of my studies and who unfortunately passed away in May 2016. I dedicate this work to him.

Abstract

Title of the thesis: **Optimalisation of track reconstruction using vertex detector in the NA61/SHINE experiment**

The main result of this thesis shows the first direct measurement of open charm hadrons (D^0 and $\overline{D^0}$) in the collisions of nuclei at the top energy of Super Proton Synchrotron (SPS). It was obtained from the data collected by the NA61/SHINE experiment and is the final result of the feasibility studies of new NA61/SHINE physics programme. The programme of charm measurements was motivated by the following questions:

- What is the mechanism of open charm production?
- How does the onset of deconfinement impact open charm production?
- How does the formation of quark-gluon plasma impact J/ψ production?

To answer these questions, one need to know the mean number of charm quark pairs $\langle c\bar{c} \rangle$ produced in a full phase space in heavy-ion collisions. Up to now, such a data does not exist and NA61/SHINE started the corresponding measurements in December 2016. Because of very short lifetime of open charm hadrons, a micro vertex detector is needed to perform the measurement. In December 2016, the Small-Acceptance Vertex Detector (SAVD) was installed and the first data for Pb+Pb collisions at $150A$ GeV/c were collected. The Vertex Detector will be upgraded during the Long Shutdown 2 at CERN (2019-2020).

The first step of the data analysis was reconstruction. Two algorithms implemented as a part of this thesis were used: the algorithm of silicon sensors alignment and the algorithm of VD-TPC track matching. The geometry corrections were calculated in a way to minimise the distances between clusters and fitted tracks. The data collected without magnetic field were used, because then clusters created by one particle should lie on the straight line. The final corrections improved the spatial clusters resolution up to 20%. The track matching was done using the method via interpolation. At first the tracks were refitted to primary vertex reconstructed by Vertex Detector (for primary tracks) or to VD cluster from second station (for secondary tracks) and then interpolated to VD stations in order to collect the matching clusters.

The implemented algorithms were tested on the analysis of K^0_s signal. The signal was successfully observed but the analysis showed the calibration problem of a part of the collected collisions. Thus, for the final analysis only properly calibrated data were used. As the most important result, the invariant mass distribution of reconstructed secondary tracks was obtained, assuming the pion and kaon masses. It shows the indication of D^0 and $\overline{D^0}$ signal reconstructed from the decay channel: $D^0 \rightarrow \pi^+ + K^-$. This result allowed to validate the measurement concept and confirmed that NA61/SHINE is able to measure open charm hadrons.

Keywords:
CERN, NA61/SHINE, quark-gluon plasma, vertex detector, open charm

(podpis opiekuna naukowego)   (podpis dyplomanta)

Streszczenie

Tytuł pracy: **Optymalizacja rekonstrukcji śladów cząstek z wykorzystaniem detektora wierzchołka w eksperymencie NA61/SHINE**

Głównym wynikiem poniższej pracy magisterskiej jest pierwszy bezpośredni pomiar otwartego powabu (D^0 i $\overline{D^0}$) w zderzeniach ciężkich jonów przy energiach akceleratora Super Proton Synchrotron (SPS) w ośrodku CERN. Został on uzyskany z analizy danych zebranych przez eksperyment NA61/SHINE i stanowi końcowy wynik studium wykonalności przyszłego programu fizycznego tegoż eksperymentu. Nowy program fizyczny motywowany jest trzema głównymi pytaniami:

- Jaki jest mechanizm produkcji otwartego powabu?
- Jak efekt uwolnienia kwarków wpływa na produkcję otwartego powabu?
- Jak wytworzenie plazmy kwarkowo-gluonowej wpływa na produkcję mezonów J/ψ?

Aby udzielić odpowiedzi na powyższe pytania, niezbędna jest znajomość średniej krotności par powabnych kwarków $\langle c\bar{c} \rangle$ produkowanych w pełnej przestrzeni fazowej, w zderzeniach ciężkich jonów. Dotychczas takie dane nie były dostępne. Ze względu na bardzo krótki czas życia hadronów z otwartym powabem, do ich pomiaru niezbędny jest precyzyjny detektor wierzchołka. W grudniu 2016 zainstalowano detektor wierzchołka małej akceptancji (Small-Acceptance Vertex Detector – SAVD) i przy jego pomocy zebrano pierwsze dane dla zderzeń Pb+Pb przy pędzie wiązki 150A GeV/c.

Pierwszym etapem analizy zebranych danych jest rekonstrukcja. W tym celu wykorzystano 2 algorytmy zaimplementowane w ramach omawianej pracy; algorytm pozycjonowania krzemowych sensorów oraz algorytm łączenia śladów cząstek zrekonstruowanych przy pomocy detektora wierzchołka ze śladami z innych poddetektorów spektrometru NA61/SHINE. Korekcję na położenia sensorów, obliczono minimalizując odległości między zrekonstruowanymi śladami oraz zebranymi klastrami. Po zastosowaniu korekcji, rozdzielczość położenia klastrów polepszyła się do 20%. Do łączenia zrekonstruowanych śladów wykorzystano metodę bazującą na interpolacji. W pierwszym etapie ślad jest ponownie dopasowywany uwzględniając położenie wierzchołka zrekonstruowanego z detektora wierzchołka (w przypadku śladów pierwotnych) lub położenie klastra z drugiej stacji detektora wierzchołka (dla śladów wtórnych). Następnie ślad jest interpolowany do pozostałych stacji, gdzie dobierane są pasujące klastry.

Zaimplementowane algorytmy przetestowano na analizie sygnału z rozpadu K_s^0. Odpowiedni sygnał został zaobserwowany. Analiza wykazała jednak problemy z kalibracją części zebranych danych. Dlatego, do końcowej analizy wykorzystano tylko dane poprawnie skalibrowane. Jako najważniejszy wynik pracy, otrzymano rozkład masy niezmienniczej zrekonstruowanych śladów wtórnych, zakładając masę pionu i kaonu. Na rozkładzie widoczny jest wyraźny sygnał z rozpadu mezonów D^0 i $\overline{D^0}$. Otrzymany wynik potwierdza koncept samego pomiaru, jak również zdolność eksperymentu NA61/SHINE do analizy produkcji otwartego powabu, co jest głównym celem eksperymentu po 2020 roku.

Słowa kluczowe:

CERN, NA61/SHINE, plazma kwarkowo-gluonowa, detektor wierzchołka, otwarty powab

(podpis opiekuna naukowego)   (podpis dyplomanta)

Politechnika Warszawska

Wojciech Bryliński

261553

Fizyka Techniczna

Oświadczenie

Świadomy odpowiedzialności karnej za składanie fałszywych zeznań oświadczam, że niniejsza praca dyplomowa została napisana przeze mnie samodzielnie, pod opieką kierującego pracą dyplomową.

Jednocześnie oświadczam, że:

- niniejsza praca dyplomowa nie narusza praw autorskich w rozumieniu ustawy z dnia 4 lutego 1994 roku o prawie autorskim i prawach pokrewnych (Dz.U. z 2006 r. Nr 90, poz. 631 z późn. zm.) oraz dóbr osobistych chronionych prawem cywilnym,
- niniejsza praca dyplomowa nie zawiera danych i informacji, które uzyskałem/-am w sposób niedozwolony,
- niniejsza praca dyplomowa nie była wcześniej podstawą żadnej innej urzędowej procedury związanej z nadawaniem dyplomów lub tytułów zawodowych,
- wszystkie informacje umieszczone w niniejszej pracy, uzyskane ze źródeł pisanych i elektronicznych, zostały udokumentowane w wykazie literatury odpowiednimi odnośnikami,
- znam regulacje prawne Politechniki Warszawskiej w sprawie zarządzania prawami autorskimi i prawami pokrewnymi, prawami własności przemysłowej oraz zasadami komercjalizacji.

Oświadczam, że treść pracy dyplomowej w wersji drukowanej, treść pracy dyplomowej zawartej na nośniku elektronicznym (płycie kompaktowej) oraz treść pracy dyplomowej w module APD systemu USOS są identyczne.

Warszawa, dnia 02.08.2018   (podpis dyplomanta)

Oświadczenie o udzieleniu Uczelni licencji do pracy

Politechnika Warszawska

Wojciech Bryliński

261553

Fizyka Techniczna

Oświadczam, że zachowując moje prawa autorskie udzielam Politechnice Warszawskiej nieograniczonej w czasie, nieodpłatnej licencji wyłącznej do korzystania z przedstawionej dokumentacji pracy dyplomowej w zakresie jej publicznego udostępniania i rozpowszechniania w wersji drukowanej i elektronicznej*.

Warszawa, dnia 02.08.2018   (podpis dyplomanta)

---

*Na podstawie Ustawy z dnia 27 lipca 2005 r. Prawo o szkolnictwie wyższym (Dz.U. 2005 nr 164 poz. 1365) Art. 239. oraz Ustawy z dnia 4 lutego 1994 r. o prawie autorskim i prawach pokrewnych (Dz.U. z 2000 r. Nr 80, poz. 904, z późn. zm.) Art. 15a. "Uczelni w rozumieniu przepisów o szkolnictwie wyższym przysługuje pierwszeństwo w opublikowaniu pracy dyplomowej studenta. Jeżeli uczelnia nie opublikowała pracy dyplomowej w ciągu 6 miesięcy od jej obrony, student, który ją przygotował, może ją opublikować, chyba że praca dyplomowa jest częścią utworu zbiorowego."

Contents

1.   Introduction and motivation

The aim of the work described in this thesis was to find the first indication of D^0 and $\overline{D^0}$ signal in heavy-ion collisions at the Super Proton Synchrotron (SPS) energies from the direct measurement using new NA61/SHINE Small-Acceptance Vertex Detector. This is the crucial aspect of the feasibility studies of future physics programme of NA61/SHINE. As a part of this thesis, two algorithms used for the data reconstruction were implemented; the algorithm of silicon sensors alignment and the algorithm of VD-TPC track matching via interpolation. Both algorithms were tested on data collected in December 2016 for Pb+Pb collisions at 150A GeV/c. The analysis of reconstructed data was also prepared and the final result of invariant mass distribution showing D^0 and $\overline{D^0}$ peak was obtained. The result confirms that NA61/SHINE is able to perform the direct measurement of open charm hadrons, what is the main goal of the new physics programme of the experiment.

Section 2 describes the basics of Heavy-Ion Physics. At first, the Standard Model is briefly introduced. Then purpose of the studies of heavy-ion collisions is discussed. Section 3 introduces the NA61/SHINE experiment as well as the method of charm measurement. At the beginning, the current physics programme of NA61/SHINE is discussed and then the motivation of future physics programme – open charm measurements – is described. In this section also the NA61/SHINE detector is presented as well as the future plans for the upgrades. In Section 4 the data reconstruction chain algorithms, which were implemented as a part of this analysis, are described. Section 5 presents the final analysis and results. Finally, the conclusions are presented in Section 6.

2.   Heavy-Ion Physics

2.1   Standard Model

The Standard Model (SM) [1] is the quantum field theory of elementary particles and interactions between them. It was developed in 20th century by the physicists from around the world. Many predictions obtained from SM were confirmed experimentally. However, the Standard Model is not a complete theory. Firstly, it does not include the gravitational interaction. Secondly, in SM neutrinos are massless whereas there is an evidence of their mixing. It also does not include the dark matter and dark energy. Moreover, it has at least 19 free parameters which values are not predicted and has to be measured (for example the particle masses). Nevertheless, it is the most general and advanced theory ever created.

The Standard Model assumes the existence of 12 elementary particles (quarks and leptons) with half-integer spin – so called fermions, which together with their anti-particles compose the whole known matter in the Universe. The interactions between particles are carried by bosons – the

particles with integer spin. SM explains three out of four elementary interactions: strong, weak and electromagnetic. The overall picture of all particles together with their mass, electric charge and spin is presented in Figure 1.

The group of fermions consists of quarks and leptons. There are six flavors of quarks (up, down, charm, strange, top, bottom) and six leptons (electron, electron neutrino, muon, muon neutrino, tau, tau neutrino). All fermions are divided into three families, each containing two quarks and two leptons. Particles from the first family build the whole stable matter in our Universe. Each quark carries color charge (red, green, blue or anti-red, anti-green, anti-blue for anti-quarks) and only color-neutral hadrons (particles build out of quarks) can be observed. Hadrons build out of three quarks are called baryons (qqq) or anti-baryons ($\bar{q}\bar{q}\bar{q}$) and out of two quarks are called mesons ($q\bar{q}$).

The group of bosons include gauge and scalar bosons. According to the Standard Model, the following gauge bosons exist:

- gluon – the carrier of strong interactions,
- Z^0, W^+, W^- – responsible for weak interactions,
- photon – carrier of the electromagnetic interaction.

The summary of fundamental interactions is presented in Figure 2. The only fundamental scalar boson predicted by SM is Higgs boson. It is responsible for the masses of all particles. The existence of Higgs boson was confirmed by ATLAS and CMS experiments at CERN in 2012.

Figure 1: The table of all elementary particles included in the Standard Model. Figure from Ref. [2].

Property	Gravitational Interaction	Weak Interaction (Electroweak)	Electromagnetic Interaction	Strong Interaction
Acts on:	Mass – Energy	Flavor	Electric Charge	Color Charge
Particles experiencing:	All	Quarks, Leptons	Electrically Charged	Quarks, Gluons
Particles mediating:	Graviton (not yet observed)	W^+ W^- Z^0	γ	Gluons
Strength at 10^{-18} m	10^{-41}	0.8	1	25
3×10^{-17} m	10^{-41}	10^{-4}	1	60

Figure 2: The summary of fundamental interactions. Figure from Ref. [3].

The very important part of the Standard Model is Quantum Chromodynamics (QCD) which describes the nature of strong interactions. It assumes the existence of color – additional state of freedom. It is the analogical property to the electric charge in Quantum Electrodynamics (QED) theory. However, in contrast to photons – carriers of electromagnetic interactions which are electrically neutral – gluons carry color charge. This fact causes that the force of strong interactions increase with the distance between particles. This is the reason why quarks can not exist as free particles. When trying to separate two quarks, at some point the provided energy is so high that it is more beneficial from the energetic point of view to create another pair of quark and anti-quark. This effect is called confinement and is schematically presented in Figure 3. The only way to observe quasi-free quarks is to squeeze them and make the distances between them extremely small. Then the quarks interact very weakly and start behaving like free particles. Such an effect is called asymptotic freedom.
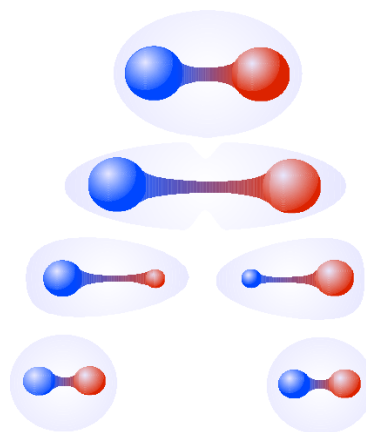

Figure 3: The schematic picture of confinement effect. Figure from Ref. [4].

2.2 Quark-gluon plasma

Quark-gluon plasma (QGP) is a state of matter in which partons (quarks and gluons) are not confined in the hadrons. The Big Bang theory predicts the formation of QGP at the very early stage of the Universe. Thus, the study of this phase of matter is one of the ways to confirm the part of the Big Bang scenario. The phase transition to QGP is expected to occur when the energy density of the system is high enough. In the laboratory, the sufficient conditions can only be achieved by colliding two particles (like heavy ions) at the appropriately high energies. The space-time evolution of such a collision is presented in Figure 4. It shows two possible scenarios; in the first one (left) the energy density is not high enough to create quark-gluon plasma. The second scenario (right) presents the collision with QGP formation. It consists of the following steps:

1. two ions approach each other and collide,

2. the non-equilibrium state is created,

3. the matter termalises and QGP is created,

4. for the whole time after the collision the system expands and cools down,

5. hadronization – quarks and gluons merge into hadrons,

6. hadron gas – quarks and gluons are confined into hadrons which interact inelastically and elastically,

7. chemical freeze-out – hadrons stop exchanging the quarks,

8. kinematic (thermal) freeze-out – the momenta of particles are fixed and the particles stop colliding with each others.
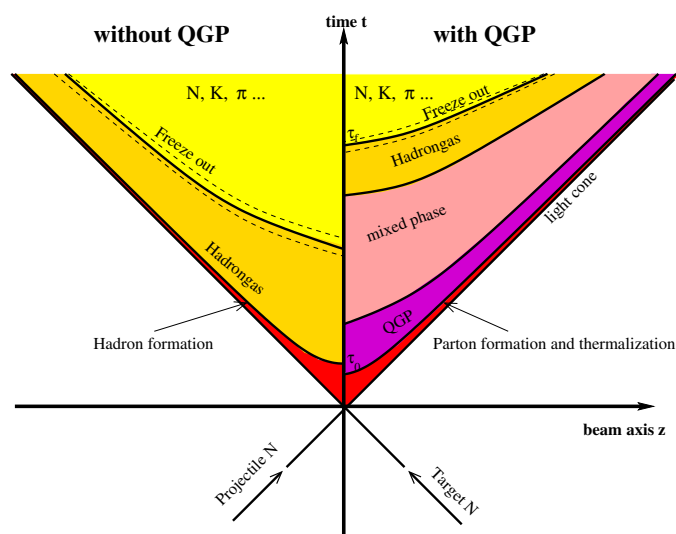
Figure 4: The space-time evolution of heavy-ion collision. Figure from Ref. [5].

The study of quark-gluon plasma properties is the main motivation of all experiments dedicated for high energy heavy-ion collisions. However, such experiments are technically able to register only the particles after the hadronization (and freezout) state. It is not possible to measure QGP directly due to its extremely high temperature, density and very short lifetime. Nevertheless, QGP can be studied by analysing some observables which are poorly sensitive to the hadronization – so-called QGP signatures. The most popular are:

- strangeness enhancement [6] – strangeness is a property of particles expressed as a quantum number. In heavy-ion collisions stragness is measured by strange hadrons. In quark-gluon plasma and hadron gas (HG) the carriers of strangeness are different; in QGP strangeness is carried by strange and anti-strange quarks while for HG the lightest strange hadrons are kaons. Thus, to produce the pair of strange carriers (due to strangeness conservation in strong interactions the s quark production must be associated with $\bar{s}$ quark production) in HG we need more energy ($2\mathrm{M}_{kaon} \approx 2 \cdot 500$ MeV, $2\mathrm{m}_s \approx 2 \cdot 100$ MeV). Moreover, comparing to the temperature of the phase transition ($\mathrm{T}_c \approx 150$ MeV at $\mu_B = 0$), strange quarks are light particles while kaons are heavy. All of these properties makes strangeness the perfect variable sensitive to the phase transition from hadron gas to quark-gluon plasma. Namely, the strangeness production should be increased in QGP scenario.

- jet quenching [7] – jets are the collimated streams of particles. Due to the conservation laws they are usually produced in di-jet structures – as two jets moving in the opposite directions. When di-jet is produced at the surface of QGP volume, one of jets (near-side) propagates normally, whereas the second one (away-side) propagates through the QGP and because of interactions with dense medium is quenched.

- charmonia suppression [8] (see Section 3.2.3) – charmonia are the bound states of charm and anti-charm quarks. The lightest one is the J/ψ meson. When quark-gluon plasma is created, the strong interactions between produced c and $\bar{c}$ quarks are screened by quark-gluon soup. Thus, it is less probable for the pair of charm quarks to stay bound and the charmonia production is expected to be suppressed.

- elliptic flow [9, 10] – the fluid-like expansion of dense matter created right after the collision. The more central collision, the more symmetrically the matter flows. In non-central collisions, the initial spatial anisotropy transfers into the pressure gradients which cause the anisotropic flow and thus the anisotropy in the momentum space. It can be studied by measuring the Fourier coefficients in the momentum distribution. The elliptic flow is measured by the second Fourier coefficient – v_2 variable. If the energy density of the collision is high enough, v_2 scales with the number of constituent quarks. This means that, the matter flows at the level of quarks and gluons what is threated as quark-gluon plasma signature.

2.3 Phase diagram of strongly interacting matter

The existing phases of strongly interacting matter (SIM) can be visualized on the phase diagram. It presents which phase is expected under the defined conditions. The phase diagram

is usually presented in the temperature - bariochemical potential (T-μ_B) coordinates system. The bariochemical potential expresses the asymmetry between baryons and anti-baryons. The higher value of μ_B, the bigger disproportion between produced matter and anti-matter. The phase diagram is shown in Figure 5. For low temperatures and bariochemical potential the hadron gas phase is expected. While increasing the temperature and μ_B the phase transition to quark-gluon plasma occurs. There are two types of phase transition predicted. For higher values of bariochemical potential the first order phase transition is expected. For $\mu_B \to 0$ the change of the character of phase transition is predicted to the smooth cross-over with the continuous (but rapid) change of physical parameters. The line of the first-order phase transition ends with the so-called critical point (CP). The experimental confirmation of CP existence would be a crucial result to verify the current predictions on the phase diagram of strongly interacting matter. However, at the time of writing this thesis the critical point has not been discovered.
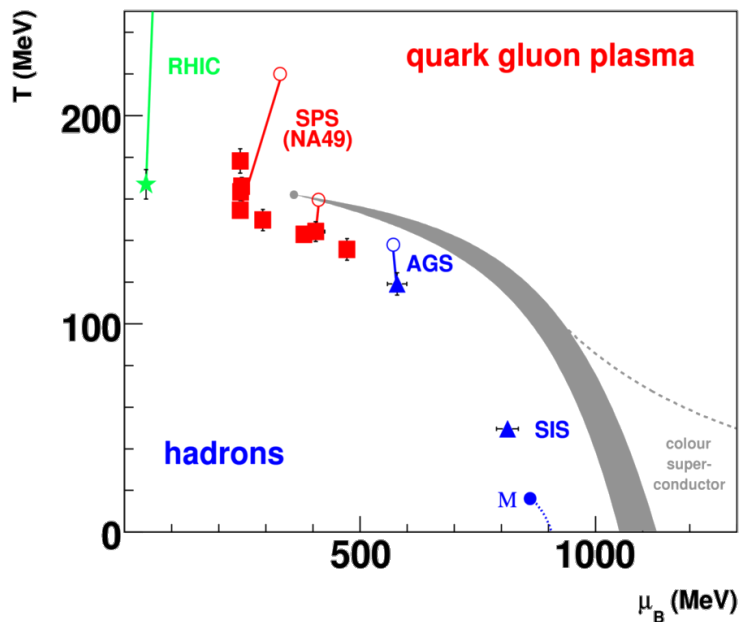
Figure 5: The phase diagram of strongly interacting matter. The gray band corresponds to the first order phase transition finished by the critical point. The close points correspond to the chemical freeze-out and open points to the hypothetical points of the early stage of the collision. Figure from Ref. [11].

3. NA61/SHINE experiment and charm measurement

SPS **H**eavy **I**on and **N**eutrino **E**xperiment (SHINE) [12, 13] is a fixed-target experiment operating at the Super Proton Synchrotron (SPS) at the European Organization for Nuclear Research (CERN). The experiment is dedicated to explore the phase diagram of strongly interacting matter. It is the next experiment after NA49 [14] from which SHINE inherited most of the subdetectors. The NA61/SHINE collaboration consists of 137 physicists from 27 institutions from 12 countries.

3.1 Current physics programme

The physics program of the NA61/SHINE experiment is focused on the following goals:
- search for the critical point of strongly interacting matter phase diagram,
- study of the properties of the onset of deconfinement [1],
- reference measurements for neutrino T2K and Fermilab programme,
- reference measurements for the Pierre Auger Observatory and KASCADE cosmic-ray experiments.

3.1.1 Two-dimensional scan of phase diagram

The main physics motivation of the NA61/SHINE experiment is to study the properties of the phase transition between hadronic matter and quark-gluon plasma. Within this program the collisions of different systems (p+p, p+Pb, Be+Be, Ar+Sc, Xe+La, Pb+Pb) at wide range of beam momenta ($13A - 150/158A$ GeV/c) are registered. Recently, in 2017, Xe+La collisions were recorded. The overall summary of collected and planned data is presented in Figure 6.
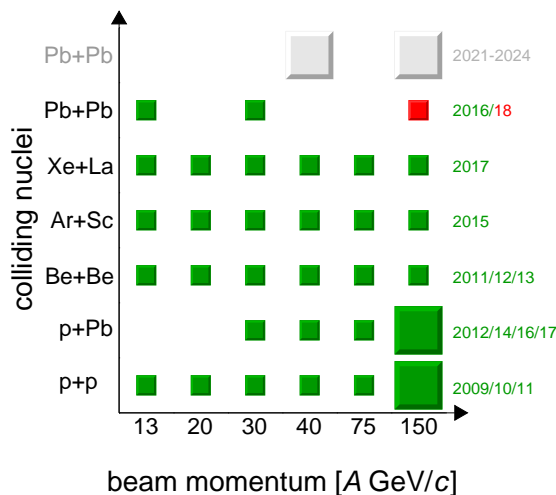
Figure 6: The schematic picture presenting the data collected within system size – beam momentum scan performed by NA61/SHINE. Figure from Ref. [15].

---

[1] minimal conditions (for example minimal energy) for which QGP can be created

The presented system size – beam momentum scan allows to cover the large area on the phase diagram of strongly interacting matter (see Section 2.3), where the critical point is expected. According to one of the QCD lattice calculations (the calculations performed on the discrete space-time lattice) the temperature and bariochemical potential at the critical point are: $T^{CP} = 162 \pm 2$ MeV, $\mu_B^{CP} = 360 \pm 40$ MeV [16]. Figure 7 presents the expected (NA61) and measured (NA49) points of chemical freeze-out on the phase diagram for NA49 and NA61 data. After collecting the data, NA61/SHINE collaboration performs the analyses looking for the signatures of critical point and studying the phase transition from HG to QGP.
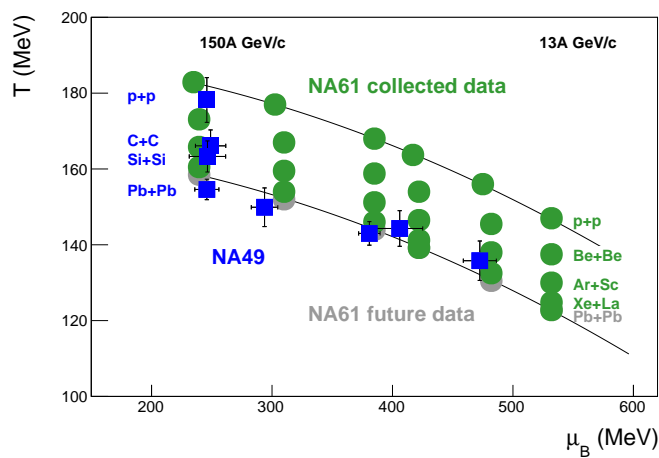
Figure 7: The coverage of the phase diagram of strongly interacting matter by NA61/SHINE data. Figure from Ref. [15].

3.2 Motivation of open charm measurements

Recently, the physics programme of the NA61/SHINE experiment was extended by the measurement of open charm hadrons (hadrons composed by one charm or anti-charm quark and light quarks/anti-quarks) at the CERN SPS energies. It was motivated by three main questions:

- What is the mechanism of open charm production?
- How does the onset of deconfinement impact open charm production?
- How does the formation of quark-gluon plasma impact J/ψ production?

In order to answer all of these three questions, the mean multiplicity of charm quarks $\langle c\bar{c}\rangle$ produced in a full phase space in heavy-ion collisions has to be known. Up to now, the corresponding data does not exist. The acceptance of the NA61/SHINE detector is large enough to extrapolate the measurements to the full phase space with relatively small uncertainties. This unique feature makes NA61/SHINE the only experiment which is able to perform such a measurement in the near future. In Sections 3.2.1, 3.2.2 and 3.2.3 the questions listed above, which motivate such studies, are illustrated on the examples.

3.2.1 Mechanism of charm production

In Figure 8 the predictions of different models on the mean multiplicity of charm quark pairs $\langle c\bar{c}\rangle$ produced in central Pb+Pb collisions at 158A GeV/c are presented. The main conclusion from the plot is that the predictions differ by about two orders of magnitude. These very different models could coexist up to now because of lack of the experimental data. Therefore, the precise measurement of $\langle c\bar{c}\rangle$ will narrow the spectrum of theoretical predictions and thus will allow to better understand the charm quarks and hadrons production mechanism.
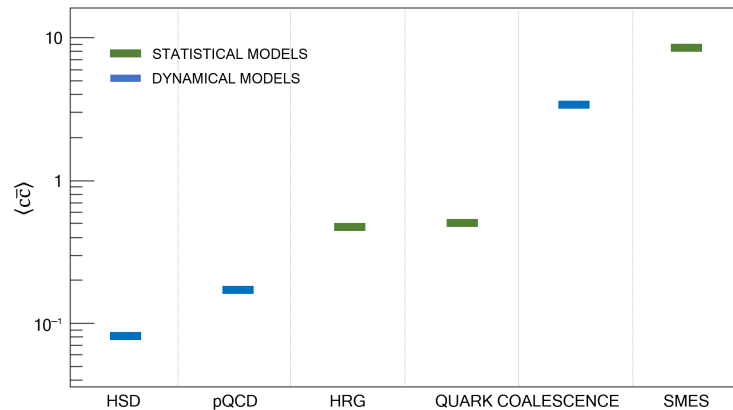
Figure 8: Mean multiplicities of charm quark pairs produced in a full phase-space in central Pb+Pb collisions at 158A GeV/c calculated within statistical models (green bars): the Hadron Resonance Gas model (HRG) [17], the Statistical Quark Coalescence model [17] and the Statistical Model of the Early Stage (SMES) [18] as well as dynamical models (blue bars): the Hadron String Dynamics (HSD) model [19, 20], a pQCD-inspired model [21, 22] and the Dynamical Quark Coalescence model [23]. Figure from Ref. [24].

3.2.2   Charm yield as the signal of deconfinement

The charm production in confined state and in quark-gluon plasma is expected to be different. It is caused by the different carriers of charm in both phases. In the hadron gas the lightest, most popular charm carriers are D mesons, while in QGP charm is carried by charm quarks. This is why the production of the pair of charm carriers in confined state ($2m_D \approx 3.7$ GeV) requires an additional energy of about 1 GeV/c in comparison to the production of the pair of charm carriers in quark-gluon plasma ($2m_c \approx 2.6$ GeV). The effective number of degrees of freedom of charm particles in both phases is similar [25]. Thus, it is expected to observe an enhancement of charm production while going from confined state to quark-gluon plasma, which can be threated as the signal of deconfinement.

The example model predictions are presented in Figures 9 and 10. Figure 9 shows the predictions of the Statistical Model of the Early Stage (SMES) [25, 26]. The energy dependence of $\langle c\bar{c} \rangle$ is plotted. According to this model, at the energy of about $\sqrt{s_{NN}} = 7 - 11$ GeV, the enhancement of charm production is expected to be observed. At $150A$ GeV/c ($\sqrt{s_{NN}} \approx 16.8$ GeV) the enhancement by a factor of about 4 is predicted (when compared to the scenario without the phase transition). Figure 10 presents the predictions of pQCD-inspired model [27]. The energy dependence of ratio of mean multiplicity of charm quarks in deconfined and confined matter is plotted. At $150A$ GeV/c the enhancement by a factor of about 3 is expected.

The measurement of the mean multiplicity of charm quarks $\langle c\bar{c} \rangle$ will allow to verify the results predicted by these two different models and check whether the charm yield can be used as the signal of deconfinement.
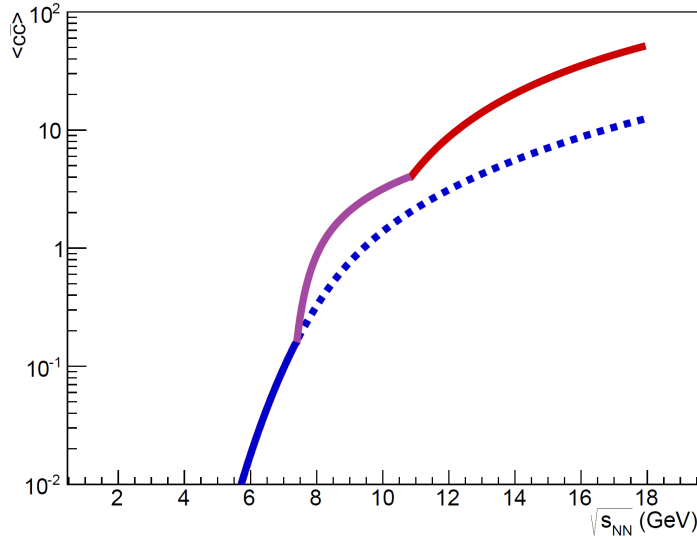
Figure 9: Energy dependence ($\sqrt{s_{NN}}$ – center of mass energy per nucleon pair) of mean multiplicity of charm quark pairs according to the Statistical Model of the Early Stage [25, 26]. Dotted line represents scenario without phase transition and solid one with phase transition (the energy of the onset of deconfinement is approximately $\sqrt{s_{NN}} \approx 7$ GeV). Figure from Ref. [24].
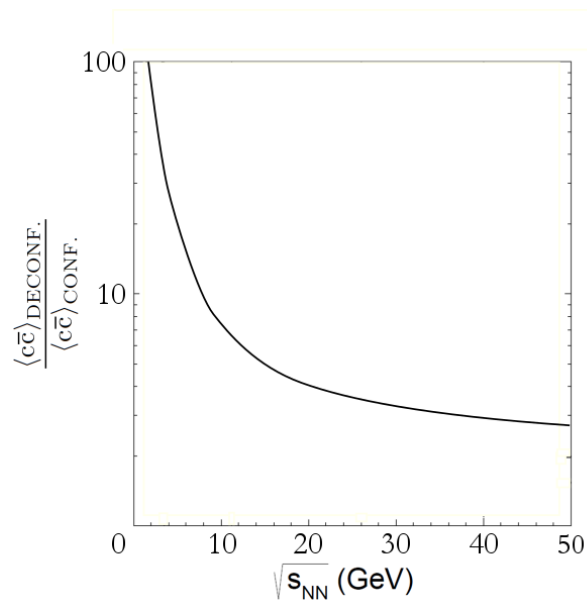
Figure 10: Energy dependence of the ratio of mean multiplicity of charm quark pairs in deconfined and confined matter in central Pb+Pb collisions calculated within the pQCD-inspired model [27]. Figure from Ref. [24].

3.2.3 J/ψ suppression as the signal of deconfinement

The J/ψ suppression is historically very important because it was strong argument for the discovery of a new state of matter announced by CERN [28]. It is explained within the Matsui-Satz model [8] as a consequence of quark-gluon plasma formation. Two scenarios of charmonia production are schematically shown in Figure 11. The first one (left) corresponds to p+p collisions when the produced $c\bar{c}$ pairs hadronize in vacuum. At high energy collisions it is expected to observe about 10% of total charm produced as charmonia and about 90% as open charm. At the second scenario (right) the strong interactions between c and $\bar{c}$ quarks are screened by other quarks and gluons. Thus, the probability that c and $\bar{c}$ quarks will stay bound decreases, what results in the decrease of the probability of J/ψ production.
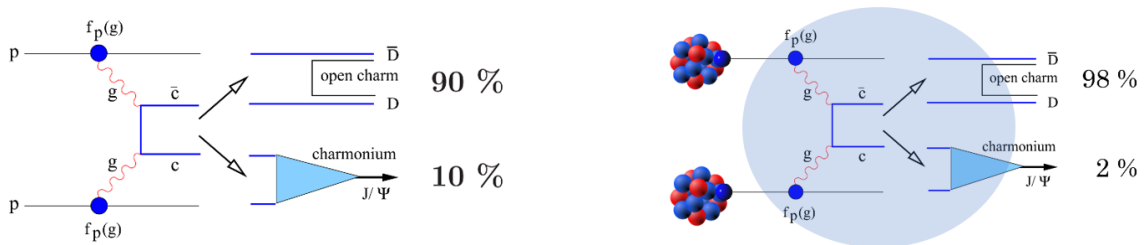
Figure 11: Schematic picture of charm production in p+p collisions (*Left*) and heavy-ion collisions (*Right*). Figure from Ref. [29].

The probability of J/ψ production is given by the following formula:

$$P(c\bar{c} \to J/\psi) \equiv \frac{\langle J/\psi \rangle}{\langle c\bar{c} \rangle} \equiv \frac{\sigma_{J/\psi}}{\sigma_{c\bar{c}}}, \tag{1}$$

where $\langle ... \rangle$ represents mean multiplicities and σ – corresponding cross-sections. Thus, in order to calculate the probability of a $c\bar{c}$ pair hadronizing to J/ψ, the data on the mean multiplicity of both J/ψ and $c\bar{c}$ in a full phase space is required. The J/ψ yields were precisely measured by other SPS experiments (NA38 [30], NA50 [31], NA60 [32]), while $\langle c\bar{c} \rangle$ was not measured before – NA61/SHINE started the corresponding measurements in 2016.

Up to now, in order to analyse very rich J/ψ measurements, the assumption that the mean multiplicity of $c\bar{c}$ quarks is proportional to the mean multiplicity of Drell-Yan [2] pairs was used [8, 31]:

$$\langle c\bar{c} \rangle \sim \langle DY \rangle. \tag{2}$$

Based on this assumption, the NA50 experiment results, presented in Figure 12, were interpreted as the evidence of quark-gluon plasma formation in central (with large transverse energy E_T) Pb+Pb collisions at 158A GeV/c. However, such a conclusion is based on the assumption which may be incorrect. The precise measurement of $\langle c\bar{c} \rangle$ will allow to verify the assumption and make much stronger conclusion on this very important result.
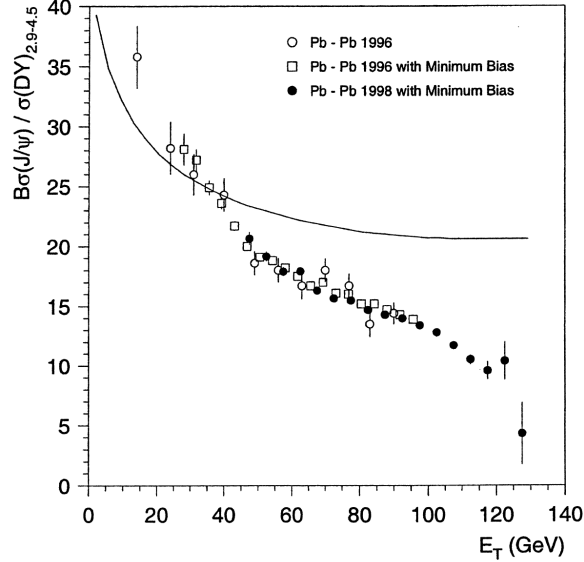
Figure 12: The branching ratio (B) multiplied $\sigma_{J/\psi}$ and divided by σ_{DY} as a function of transverse energy (measure of collision centrality) in Pb+Pb collisions at 158A GeV/c measured by NA50. The curve represents the J/ψ suppression due to ordinary ("cold") nuclear matter absorption. Figure from Ref. [31].

---

[2]process of production of the lepton pair in hard (with large momentum transfer), electromagnetic hadron interactions

3.3   Idea of open charm measurements

In order to estimate the mean multiplicity of charm quarks $\langle c\bar{c} \rangle$, the yields of all the most popular charm carriers need to be known. The distribution of open charm among charm carriers is presented in Figure 13. According to Parton Hadron String Dynamics (PHSD) model predictions [19, 20], the largest fraction of total charm is contained in D^0 mesons. This is the reason why the NA61/SHINE collaboration first focused on D^0 signal reconstruction as the test measurement. However, after the necessary upgrades of NA61/SHINE detectors (see Section 3.5.1), the collaboration will be able to measure the yields of all most abundant charm hadrons what will give the first direct measurement of $\langle c\bar{c} \rangle$ at the SPS energies. The hadrons for which the measurement will be performed, together with their lifetimes, reconstructable decay channels and their branching ratios, are listed in Table 1.
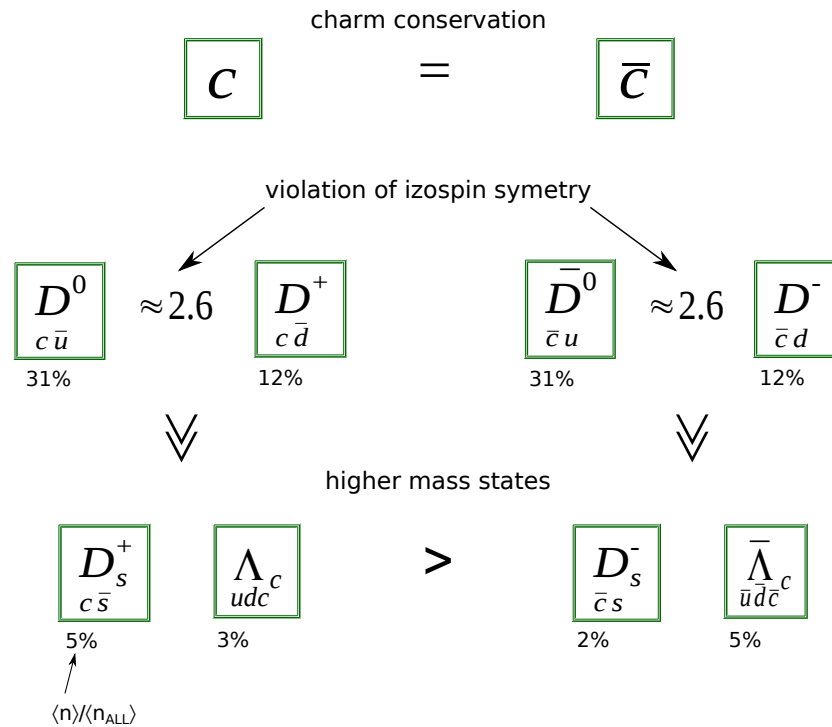
Figure 13: Total charm distribution over different charm hadrons according to PHSD model [19, 20] for Pb+Pb collisions at 158A GeV/c.

The whole measurement is very hard due to short lifetime of charm particles and low branching ratios into reconstructable decay channels. The D^0 meson lifetime is equal to about 410 fs, which corresponds to the distance of about 123 μm. Since NA61/SHINE is a fixed-target experiment, due to the Lorenz boost, the average separation between primary vertex and vertices of D^0 decays is equal to about 1 mm. This makes the measurement significantly easier than in case of collider experiments.

Table 1: The most frequently produced charm hadrons: their mass, mean lifetime multiplied by the speed of light and the decay channel (with its branching ratio BR) best suited for measurements are shown. Numerical values are taken from Ref. [33].

Hadron	Mass [MeV]	$c\bar{\tau}$ [μm]	Decay channel	BR
D^0	1864.83 ± 0.05	123	$\pi^+ + K^-$	3.89%
D^+	1869.65 ± 0.05	312	$\pi^+ + \pi^+ + K^-$	9.22%
D_S^+	1968.34 ± 0.07	150	$\pi^+ + K^- + K^+$	5.50%
Λ_c	2286.46 ± 0.14	60	$p + \pi^+ + K^-$	5.00%

However, additional tracking device (Vertex Detector) is needed to be able to distinguish between primary and the decay vertices of D^0 mesons. The schematic idea of D^0 measurement is presented in Figure 14.
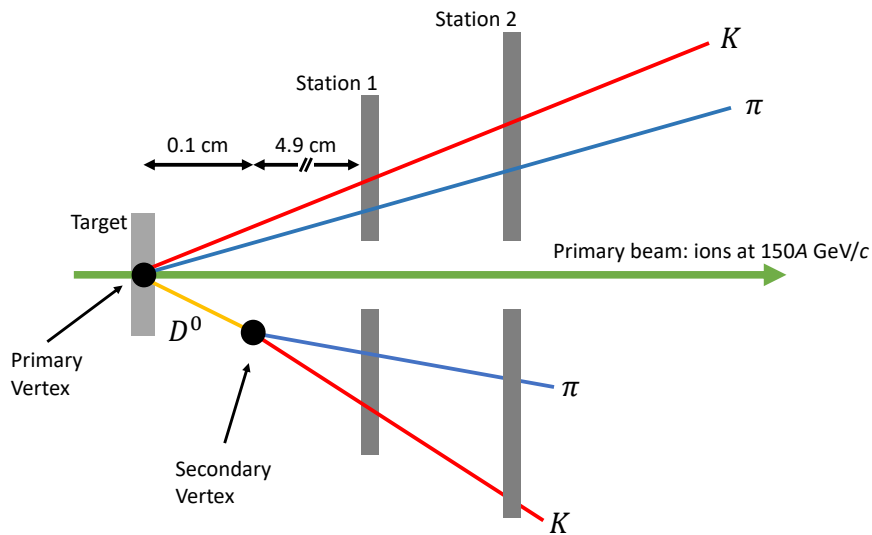
Figure 14: The schematic picture showing the idea behind D^0 meson measurement. Figure from Ref. [24].

3.4 NA61/SHINE detector

The NA61/SHINE detector is a multi-purpose spectrometer optimised to study hadron production in different types of collisions: p+p, h+A (hadron+nucleus), A+A (nucleus+nucleus). The schematic picture of the detector is presented in Figure 15. The main subdetectors of the whole setup are Time Projection Chambers. Two of them (Vertex-TPCs, VTPCs) located in the magnetic field together with two large volume Main-TPCs (MTPCs) are main tracking devices. There are also smaller TPCs: GAP-TPC and 3 Forward-TPCs (FTPCs) located along the beam axis. Such a setup gives an excellent capabilities in charged particles momenta measurement and allows for the particle identification complimented by the information from the Time-of-Flight (ToF) detectors. The last detector on the beamline is Projectile Spectator Detector (PSD), which measures the energy of spectators – non-interaction nucleons. This information is used to determine the centrality in A+A collisions. Beam particles are measured by an array of beam detectors. They are used for the trajectory measurement as well as the identification of primary (from SPS) and secondary (from fragmentation) hadrons and ions. The signal from these detectors is also used for triggering the data acquisition. In 2016, the whole spectrometer was upgraded by adding Vertex Detector (SAVD) which is described in details in Section 3.4.1.
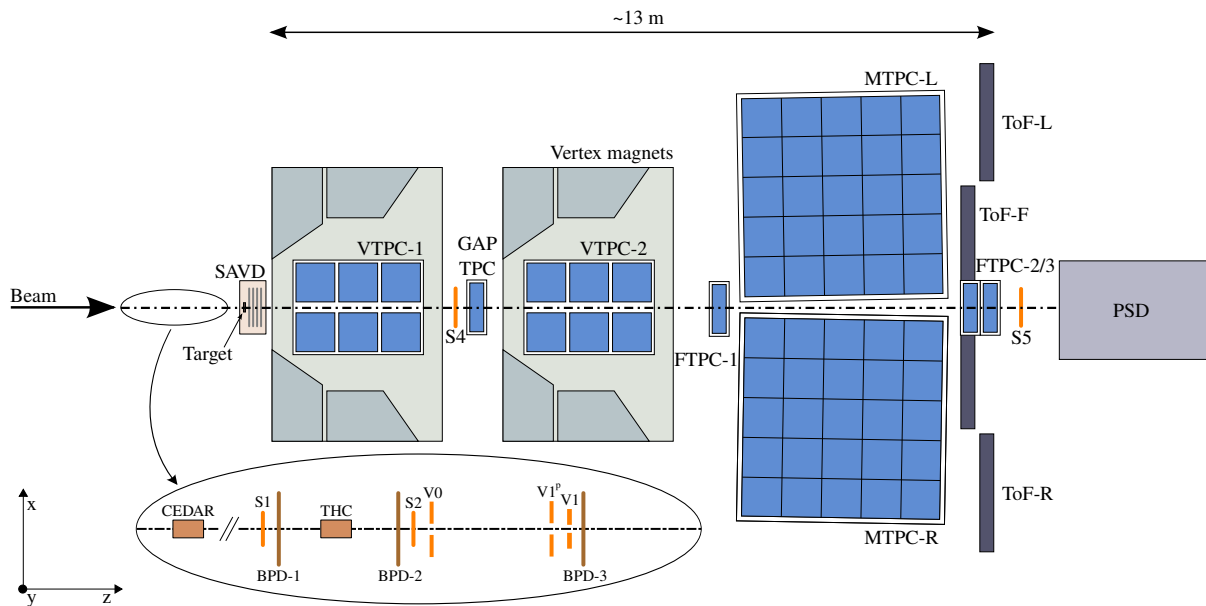
Figure 15: The schematic picture of the NA61/SHINE detector. Figure from Ref. [15].

3.4.1 Small-Acceptance Vertex Detector

In order to meet the challenges of required spatial resolution of reconstructed primary and secondary vertices (see Section 3.3), the NA61/SHINE detector was upgraded with Vertex Detector (VD). In December 2016, the test version – Small-Acceptance Vertex Detector (SAVD) – was successfully commissioned and first Pb+Pb collisions were registered. SAVD is build out of 16 MIMOSA-26 silicon sensors [34] located in two movable arms. The basic properties of used silicon sensors are:

- 1152x576 pixels of 18.4x18.4 μm^2
- readout time: 115.2 μs
- 50 μm thin

The target holder was integrated with the whole system. Figure 16 shows the final project of the Small-Acceptance Vertex Detector (*Left*) as well as the photo of constructed SAVD (*Right*).

Figure 16: The final project (*Left*) and the photo (*Right*) of the Small-Acceptance Vertex Detector. Figure from Ref. [24].

According to A Multi-Phase Transport Model (AMPT) [35] simulations, using data collected with Small-Acceptance Vertex Detector after the analysis cuts, it is possible to reconstruct about 5% of all D^0 decays in decay channel: $D^0 \rightarrow \pi^+ + K^-$. The phase-space coverage of SAVD is presented in Figure 17.
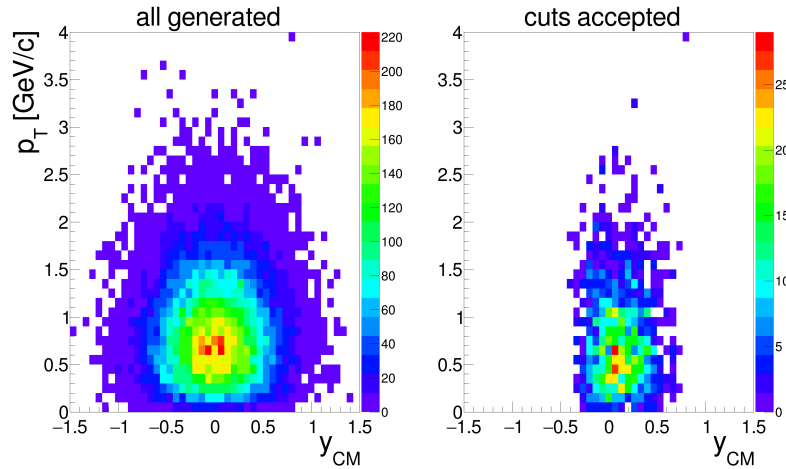
Figure 17: Transverse momentum (momentum in plane perpendicular to beam axis) and rapidity ($y = \frac{1}{2}\ln\frac{E+p_L}{E-p_L}$, where: E – energy, $p_L = p_z$ – momentum along z axis; y_{CM} – rapidity calculated in center-of-mass frame) distributions of $D^0 + \overline{D^0}$ mesons produced in central Pb+Pb collisions at 150A GeV/c simulated within the AMPT model and corresponding to $3 \cdot 10^6$ events. *Left*: Results for all produced $D^0 + \overline{D^0}$ mesons. *Right*: results for $D^0 + \overline{D^0}$ mesons fulfilling the following criteria: decay $D^0 \to \pi^+ + K^-$ and $\overline{D^0} \to \pi^- + K^+$, both decay products registered by the SAVD, passing background suppression and quality cuts [36]. Figure from Ref. [24].

3.5 NA61/SHINE beyond 2020

Although the feasibility studies on charm were already performed, the precise measurements of charm hadrons production at the SPS energies are expected to be done in 2022-2024. For this purpose, during the Long Shutdown 2 at CERN (2019-2020), the NA61/SHINE detector will be significantly upgraded [24]. The plans of the upgrade are presented in Section 3.5.1. From the point of view of charm physics programme, the most important upgrade concerns the NA61/SHINE Vertex Detector. This upgrade is discussed in Section 3.5.2.

3.5.1 NA61/SHINE detector upgrades

During the Long Shutdown 2 at CERN (2019-2020), the NA61/SHINE spectrometer is planned to be upgraded [24]. Most of the upgrades are dedicated to the charm physics programme which requires the increase of the phase-space coverage of Vertex Detector and the tenfold increase of data taking rate to about 1 kHz. To obtain the required goals, the following is planned to be done:

- construction of new NA61/SHINE Vertex Detector,
- replacement of TPC read-out electronics,
- preparing new data acquisition and trigger system,
- update of Projectile Spectator Detector.

Additionally, new Time-of-Flight detectors will be constructed to improve the particle identification in mid-rapidity (central region of rapidity).

The overall picture of all upgrades is presented in Figure 18.

Construction of Vertex Detector (VD)
for D^0, $\overline{D^0}$ decay reconstruction

Replacement of the TPC
read-out electronics
to increase data rate to 1 kHz

New trigger and data
acquisition system

New Time-of-Flight
detectors

Upgrade of Projectile
Spectator Detector
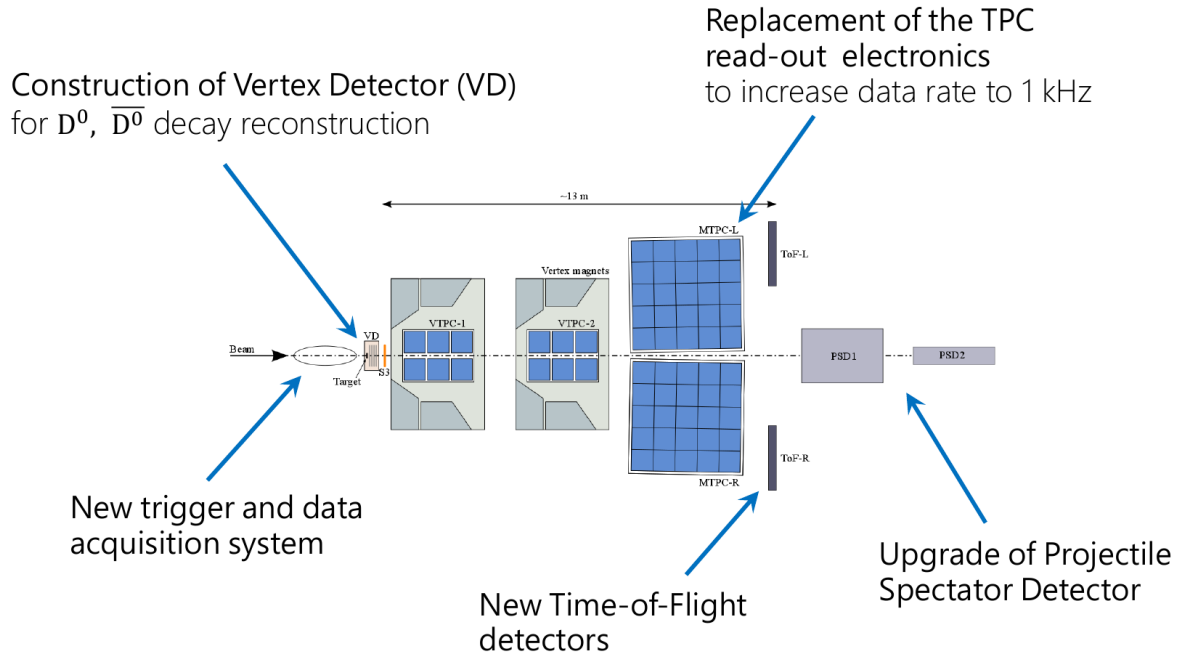
Figure 18: Summary picture of all upgrade plans of the NA61/SHINE detector. Figure from Ref. [24].

3.5.2   NA61/SHINE Vertex Detector

The main upgrade for charm physics programme is the construction of NA61/SHINE Vertex Detector (VD). The collaboration decided to use the technology developed by the ALICE group – the ALPIDE [37] silicon sensors. The main reason is the fact of much lower noise in comparison to MIMOSA-26 sensors used for SAVD (see Section 3.4.1). The read-out time is also smaller for ALPIDE sensors what allows to increase the data taking rate to the planned value (see Section 3.5.1). The final layout of the Vertex Detector is presented in Figure 19 and 20.
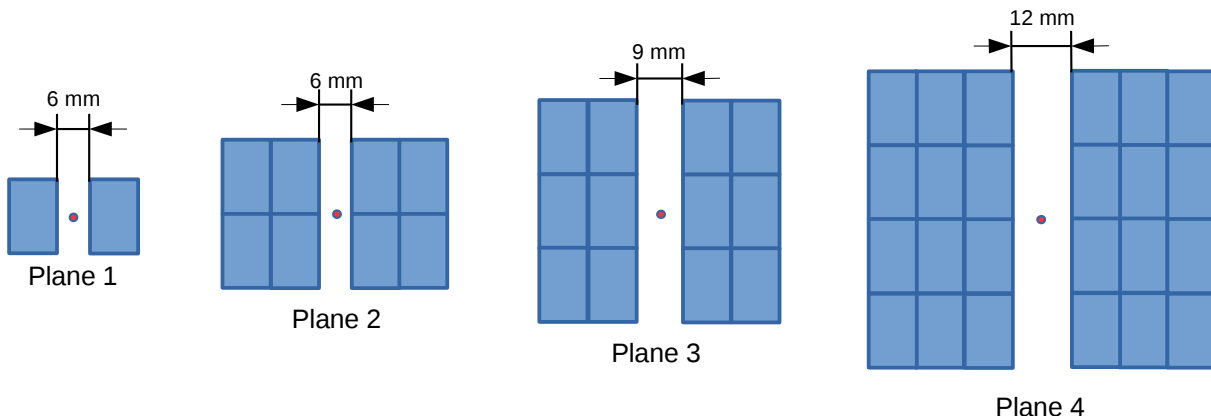
Figure 19: The picture of the layers of VD based on the ALPIDE sensors. From left to right: the first layer with two sensors, the second layer with 8 sensors, the third layer with 12 sensors and the fourth layer with 24 sensors. The total active area of the VD sensors is 190 cm^2. Figure from Ref. [24].
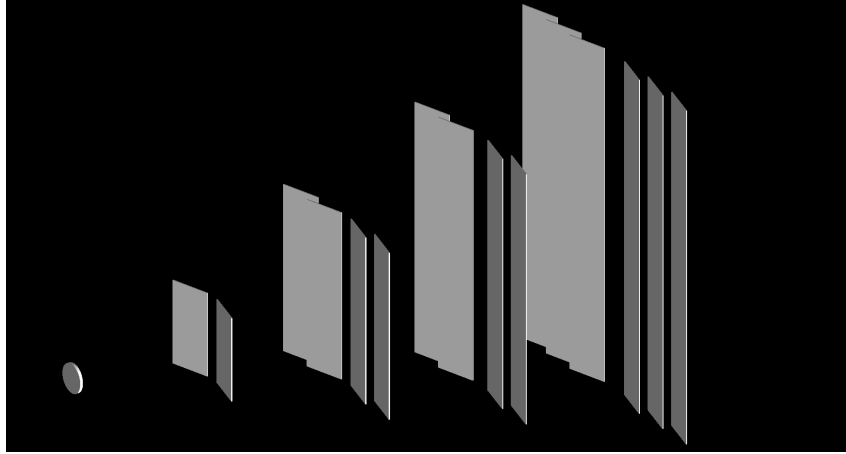
Figure 20: The 3D visualization of the VD geometry presented in Fig. 19. Figure from Ref. [24].

According to AMPT simulations, the NA61/SHINE Vertex Detector will be able to reconstruct about 13% (about 3 times more than for SAVD) of all D^0 decays in decay channel: $D^0 \to \pi^+ + K^-$ and about 9% of all D^+ decays in decay channel: $D^+ \to \pi^+ + \pi^+ + K^-$. The phase-space coverage of VD is shown in Figure 21.
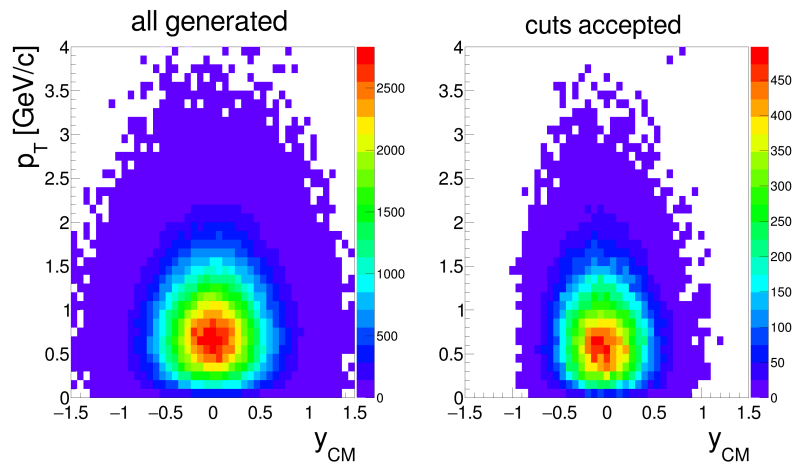
Figure 21: Transverse momentum and rapidity distributions of D^0 + $\overline{D^0}$ mesons produced in central Pb+Pb collisions at 150A GeV/c simulated within the AMPT model and corresponding to $500 \cdot 10^6$ events. *Left*: Results for all produced D^0 + $\overline{D^0}$ mesons. *Right*: results for D^0 + $\overline{D^0}$ mesons fulfilling the following criteria: decay $D^0 \to \pi^+ + K^-$ and $\overline{D^0} \to \pi^- + K^+$, both decay products registered by the future NA61/SHINE Vertex Detector, passing background suppression and quality cuts [36]. Figure from Ref. [24].

4. Data reconstruction

This thesis has a significant input to the reconstruction chain used for the data collected by Small-Acceptance Vertex Detector (see Section 3.4.1). The whole data reconstruction includes the following steps:

- geometry tuning,
- track finding,
- primary vertex reconstruction,
- SAVD-TPC track matching,

As a part of this thesis the algorithms for geometry tuning and VD-TPC track matching were implemented. These algorithms are described in Sections 4.1 and 4.2, respectively. Both algorithms were tested on Pb+Pb collisions at 150A GeV/c registered in December 2016 using SAVD, however they can be easily adapted for the future measurements which will be done using upgraded NA61/SHINE Vertex Detector (see Section 3.5.2). The track finding was performed using the combinatorial method by checking the colinearity of all possible combinations of clusters from different stations. Primary vertex was reconstructed by averaging the positions of the points corresponding to the Distance of Closest Approach (DCA – the smallest distance) between pairs of tracks.

4.1 Vertex Detector alignment

In order to optimise the spatial resolution of registered particles hits, the position of all sensors has to be known with very high precision. It would be impossible to measure the position of all sensors precisely enough before every data taking period. Even after opening and closing the arms of VD for beam tuning, the geometry is slightly changed. Thus, the only reasonable solution was to prepare the algorithm which calculates the required geometry corrections and apply them for the collected data. For this purpose the data registered without the magnetic field were used. Even before the geometry tuning it was possible to reconstruct the tracks candidates, but the efficiency was very poor. Such a reconstructed tracks candidates were used for the silicon sensors alignment. For the proper geometry, hits produced by one particle, should lie on the same straight line. In order to estimate the collinearity of 3 hits the "dev" variable was introduced:

$$\text{dev}_x = \frac{x_1 + x_3}{2} - x_2 \tag{3}$$

$$\text{dev}_y = \frac{y_1 + y_3}{2} - y_2 \tag{4}$$

where x_1, x_2, x_3 and y_1, y_2, y_3 correspond to the cluster x and y position on the first, second and third station accordingly. The meaning of "dev" variable is presented in Figure 22. For proper geometry, the distribution of "dev" for reconstructed tracks should present a narrow peak centered at zero. Thus, the algorithm of alignment should find a minimal value of the sum of squares of "dev" values by changing the position of sensors (each sensor has 6 degrees of freedom: offsets from the nominal

geometry in x, y, z coordinates and rotations along x, y, z axes). The naming convention of SAVD sensors is shown in Figure 23.
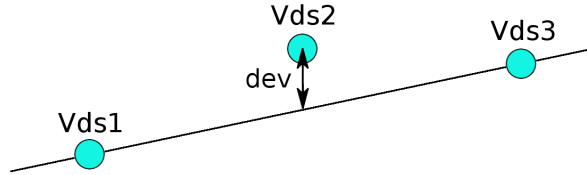
Figure 22: The definition of the "dev" variable used for geometry tuning. Vds1, Vds2 and Vds3 denote the clusters from first, second and third station of SAVD, respectively.
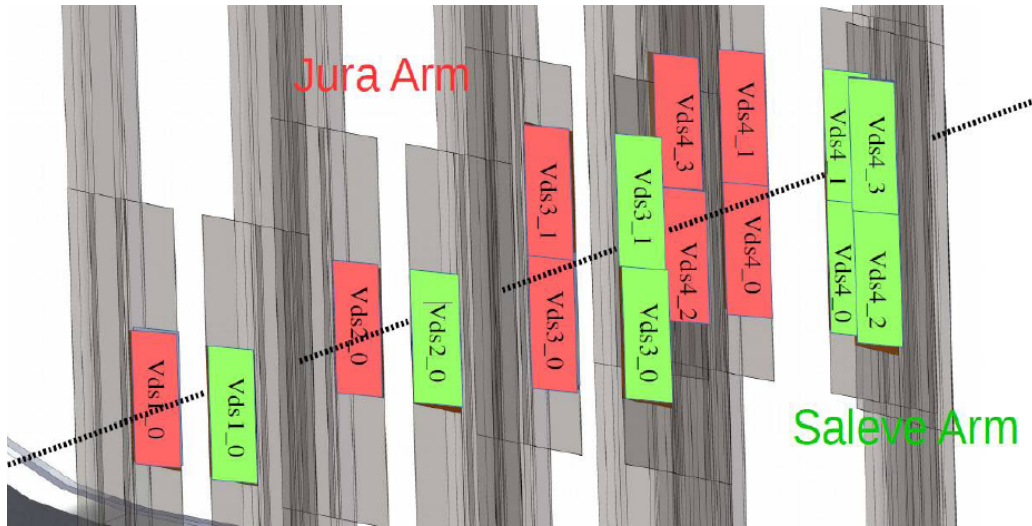
Figure 23: The naming convention of SAVD sensors. Figure from Ref. [15].

The alignment was performed separately for both arms (Jura and Saleve). For the minimisation the MIGRAD minimiser from MINUIT [38] package was used. The whole alignment algorithm consists of two main parts. The initial alignment was done as follows:

1. fix the position of the Vds1_0 sensor as the reference;

2. loop over all track candidates reconstructed from clusters registered by the following SAVD sensors: Vds1_0, Vds2_0, Vds3_0, Vds4_0;

3. calculate the sum of squares of "dev" values for clusters from stations: Vds1_0, Vds2_0, Vds3_0 and: Vds2_0, Vds3_0, Vds4_0;

4. minimise the obtained sum using the MINUIT package by slightly changing the offsets and rotations of included SAVD sensors;

5. fix the position of Vds2_0, Vds3_0, Vds4_0 sensors;

6. do the same minimisation for track candidates reconstructed from clusters registered by the following SAVD sensors: Vds1_0, Vds2_0, Vds3_1, Vds4_1;

7. fix the position of Vds3_1, Vds4_1;

8. do the analogous minimisation for track candidates reconstructed from clusters from SAVD sensors: Vds1_0, Vds2_0, Vds3_0, Vds4_2 and fix the position of the Vds4_2 sensor;

9. do the analogous minimisation for track candidates reconstructed from clusters from SAVD sensors: Vds1_0, Vds2_0, Vds3_1, Vds4_3 and fix the position of the Vds4_3 sensor.

The final alignment was done for all sensors simultaneously. Instead of "dev" variable, the distributions of residuals between fitted tracks and clusters were used. This part consists of the following steps:

1. loop over all track candidates and create the distributions of residuals between refitted tracks and clusters;

2. minimize the sum of estimators of mean and standard deviation values for all the created distributions using the MINUIT package by changing the offsets and rotations of SAVD sensors.

In order to estimate the improvement of the spatial clusters resolution after geometry tuning, the distributions of residuals between fitted tracks and clusters for all the sensors (*newGeometry*) were compared with the same distributions obtained before the geometry tuning (*oldGeometry*). The Pb+Pb collisions at 150*A* GeV/*c* registered in December 2016 were analysed. The Gaussian functions were fitted to all the distributions and the standard deviation (σ) values were used to calculate the improvement factor from the following formula:

$$\text{improvement} = \frac{\sigma_{oldGeometry} - \sigma_{newGeometry}}{\sigma_{oldGeometry}} \cdot 100\% \tag{5}$$

The sigma value (σ) corresponds to the spatial resolution of clusters position, so the improvement factor shows improvement of spatial clusters resolution after final geometry tuning. The average values of improvement factors for both arms are shown in Table 2. The example comparison of the distributions of residuals for data before and after geometry tuning is presented in Figure 24.

Sensors used for track reconstruction	Improvement Factor	
	Saleve	Jura
Vds1_0, Vds2_0, Vds3_0, Vds4_0	20.23%	19.31%
Vds1_0, Vds2_0, Vds3_1, Vds4_1	20.24%	13.05%
Vds1_0, Vds2_0, Vds3_0, Vds4_2	1.07%	–
Vds1_0, Vds2_0, Vds3_1, Vds4_3	19.77%	3.82%

Table 2: Average values of improvement factors calculated from Formula (5). The Vds4_2 sensor from Jura arm was not working properly and that is why there were no tracks reconstructed using this sensor.
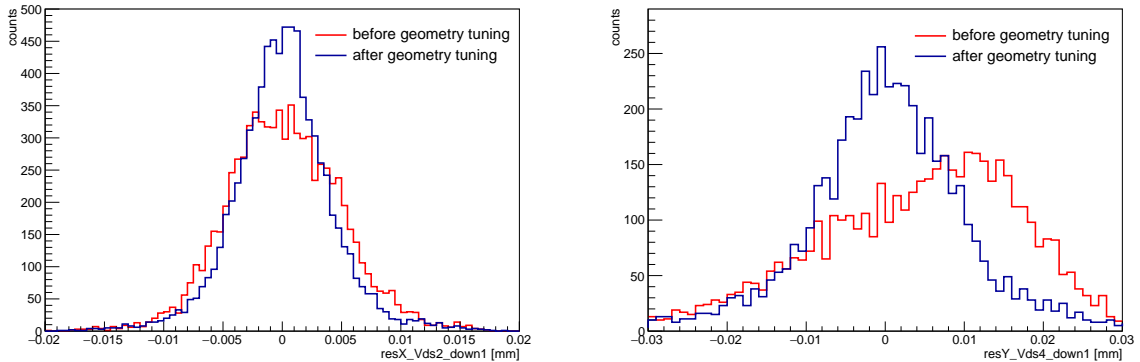
Figure 24: *Left*: The distribution of x residuals between fitted tracks and hits registered by the Vds2_0 sensor in the Jura arm. The improvement factor, calculated from Formula (5), is 20%. *Right*: The distribution of y residuals between fitted tracks and hits registered by the Vds4_0 sensor in the Saleve arm. The improvement factor, calculated from Formula (5), is 22%. Distributions before and after final geometry tuning are shown by blue and red histograms, respectively.

4.1.1 Example results

Some of the geometry corrections, calculated in the way described in Section 4.1, had unexpectedly big values. The example results for one of the sensors from Jura fourth station are listed below:

- rotations along x, y, z axes:
  - □ rotX = -0.01 (0.6°)
  - □ rotY = 0.01 (0.6°)
  - □ rotZ = -0.049 (2.8°)
- offsets from nominal geometry in x, y, z:
  - □ offsetX = 2.1 mm
  - □ offsetY = 1.1 mm
  - □ offsetZ = 0.5 mm

The photo of this sensor is presented in Figure 25. After opening SAVD for some service work, it turned out that the sensors were indeed shifted and rotated by such big values. It was caused by a problem with phase changing material (with changing temperature) which was used to glue the sensors to the ladders. This result confirms the validity of the implemented alignment algorithm.
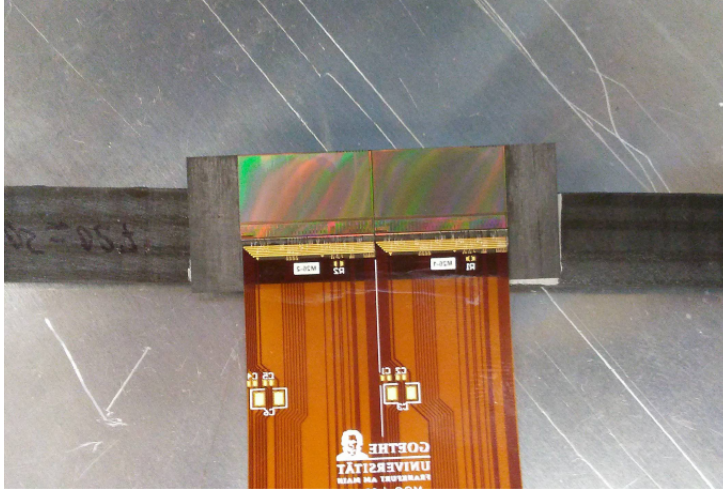
Figure 25: The photo of example rotated and shifted sensor.

4.2   VD-TPC track matching via interpolation

In order to perform the analysis of data collected using Vertex Detector, one need to match the reconstructed tracks with the tracks and information reconstructed using other subdetectors of the NA61/SHINE spectrometer (see Section 3.4). As a part of this thesis, the algorithm of matching VD tracks with TPC tracks was implemented and tested on Pb+Pb data at 150A GeV/c registered in December 2016. Because for open charm analysis only secondary tracks are needed (see Section 3.3), the matched primary tracks were not stored. The algorithm consists of the following steps:

- refit TPC track to VD primary vertex[3],

- interpolate refitted TPC track to VD stations and collect clusters,

- remove primary tracks from further analysis,

- refit TPC track to VD cluster from second station,

- interpolate refitted track to other VD stations and collect clusters,

- save secondary tracks for further analysis.

The main parts of the algorithm are described in the sections below.

4.2.1   Refitting TPC track to VD primary vertex

The first step of the track matching algorithm is to refit the track to the reconstructed VD primary vertex. For refitting the track the Kalman Filter [39] algorithm was used. The plotted example tracks before and after refitting are presented in Figure 26.

---

[3]the primary vertex reconstructed from data registered by Vertex Detector
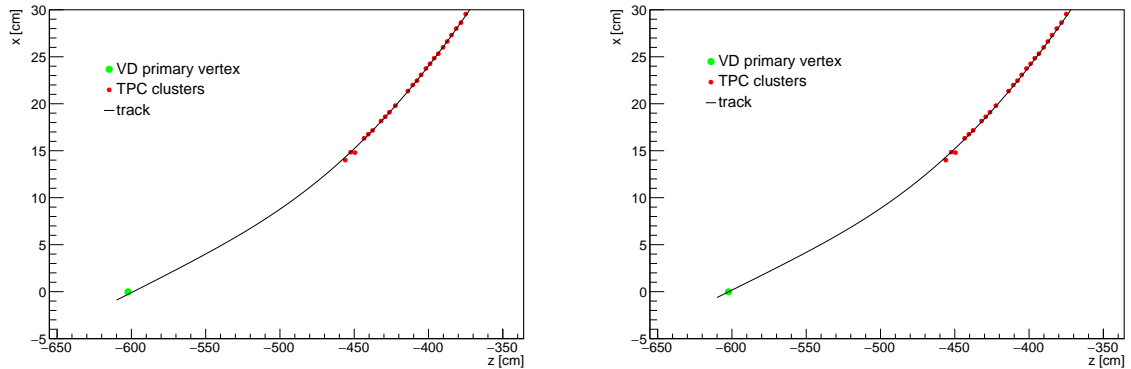
Figure 26: *Left*: Track before refitting to VD primary vertex. The vertexing precision (the uncertainty of reconstructed vertices position) from TPC reconstruction is on the order of cm. *Right*: Track after refitting to VD primary vertex. On both plots the coordinates system is as introduced in Figure 15.

4.2.2   Track interpolation to VD stations and cluster collection

As the second step, the tracks refitted to VD primary vertex were interpolated to all VD stations in order to collect the matching clusters. For every station the distribution of the distances between interpolated tracks and all VD clusters were created. The comparison of such a distribution for tracks before (left) and after (right) refitting to VD primary vertex is presented in Figure 27. The right picture shows huge combinatorial background with the correlation peak from matched tracks and clusters. For each sensor, the correlation peak was fitted with Gaussian function and the standard deviation value (σ) was used for the matching cut for primary tracks. If the distance between interpolated track and cluster is smaller than 2σ, the cluster is accepted as matched. The 2σ cut was used in order to make sure that only primary tracks were matched in this step. Finally, the track was accepted as the primary track if at least one VD cluster was matched. The example of primary track is illustrated in Figure 28.
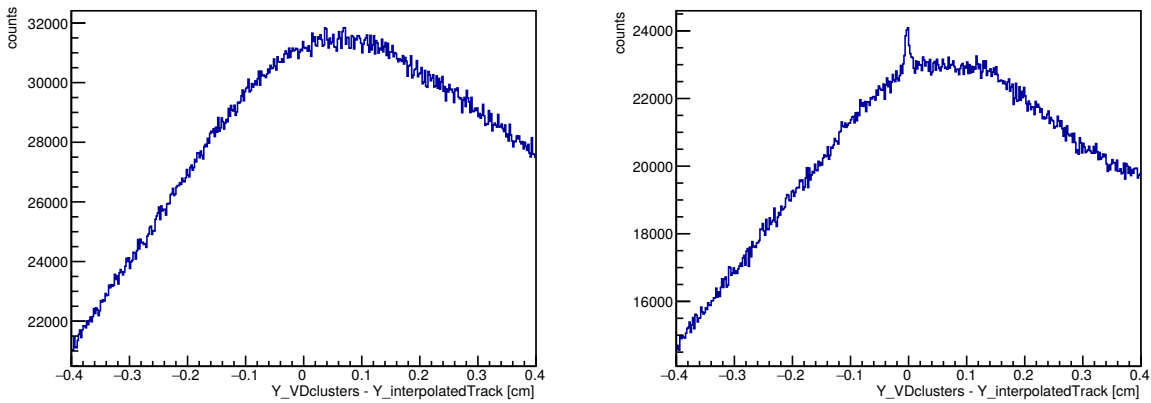
Figure 27: The distributions of the distances between interpolated tracks and all VD clusters from first station before (*Left*) and after (*Right*) refitting to VD primary vertex. It shows that in order to see the correlation between matching tracks and clusters, the first step of the algorithm (see Section 4.2.1) is needed.
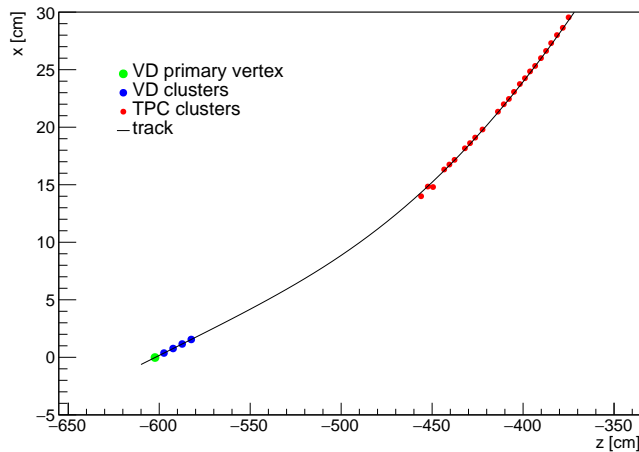
Figure 28: The matched VD clusters to TPC track.

4.2.3   Refitting TPC track to VD clusters

After removing the primary tracks, the matching algorithm for secondary tracks was performed. In the first step, each track is combined with all VD clusters from the second station. The example track before and after refitting is illustrated in Figure 29.
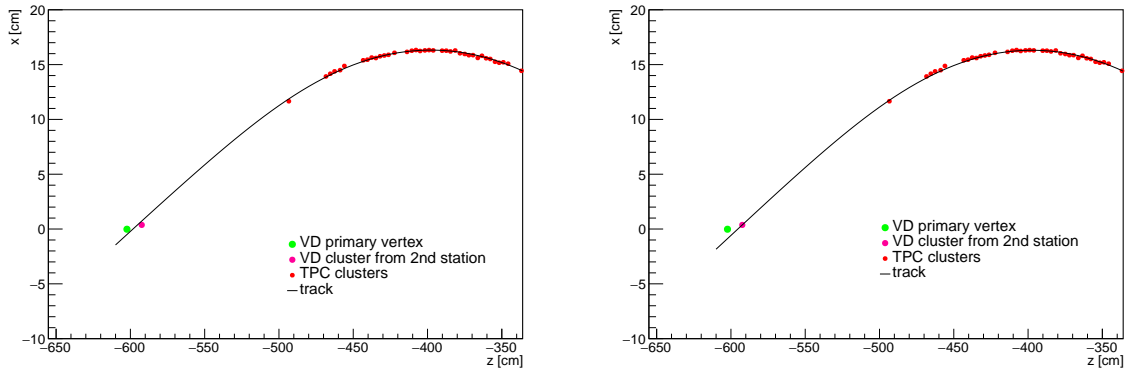
Figure 29: *Left*: Track before refitting to VD cluster. *Right*: Track after refitting to VD cluster.

4.2.4 Secondary tracks interpolation to VD stations and cluster collection

After refitting the track to the VD cluster from second station, the track is interpolated to other VD stations and the matching clusters are collected. For the matching cuts the values from primary tracks analysis are used (see Section 4.2.2). The cluster is accepted as matched if the distance from the interpolated track is smaller than 3σ. If none of VD clusters is matched, the track is refitted to the next VD cluster from the second station. The track is accepted as a secondary track if at least 3 clusters are matched (one from second station and at least two from other stations). The examples of secondary tracks are presented in Figure 30. The secondary tracks, matched in the described way, are refitted using Kalman Filter algorithm and stored for further analysis.
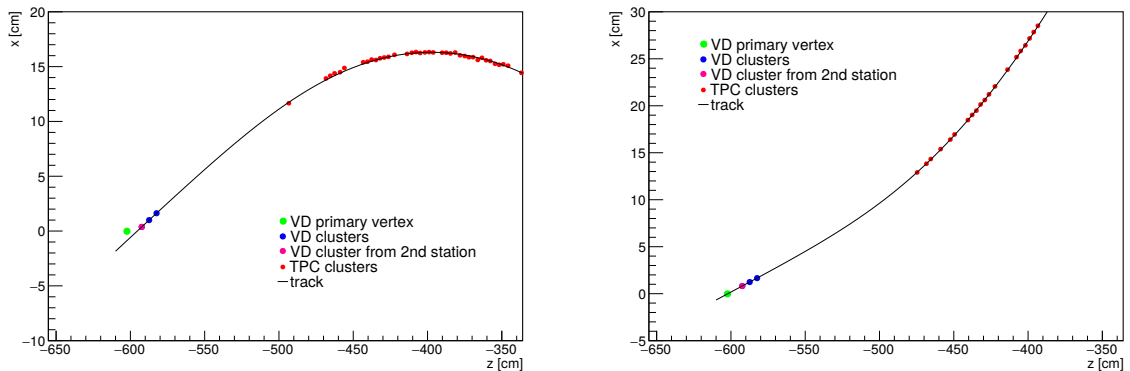
Figure 30: Example of two different secondary tracks matched with VD clusters.

5. Data analysis

In order to test the implemented reconstruction algorithms (see Section 4) the analysis of K_s^0 signal was performed. It is described in details in Section 5.1. Section 5.2 presents the $D^0 + \overline{D^0}$ signal reconstruction which is the most important result of this thesis. Both analyses were performed on Pb+Pb collisions at $150A$ GeV/c registered in December 2016.

5.1 K_s^0 test signal

The most popular decay channel of K_s^0 [4] particles is the decay into two pions ($K_s^0 \rightarrow \pi^+ + \pi^-$) with the branching ratio of 69,2%. Thus, in order to reconstruct the K_s^0 signal, all the secondary tracks reconstructed as described in Section 4.2.3 and 4.2.4 were grouped into pairs. For each pair the invariant mass of parent particle was calculated assuming the pion mass of both daughter particles and put into the histogram. The invariant mass was calculated from the following formula:

$$M_{inv} = \sqrt{(E_1 + E_2)^2 - (p_1 + p_2)^2} \qquad (6)$$

where: M_{inv} – invariant mass, E_1, E_2 – energy of first and second particle, p_1, p_2 – momentum of first and second particle. The secondary vertex was calculated as the point of closest approach between tracks. In order to reduce the combinatorial background, the cuts on the following variables were applied:

- longitudinal position of the track pair vertex relative to primary vertex: $V_z > 0 \ \mu$m,
- parent particle impact parameter (the distance between mother particle track and primary vertex): $D < 400 \ \mu$m

The value of second cut was based on D^0 analysis (see Section 5.2.1). The example distribution (for about 140k events) of reconstructed invariant mass with K_s^0 peak is presented in Figure 31.
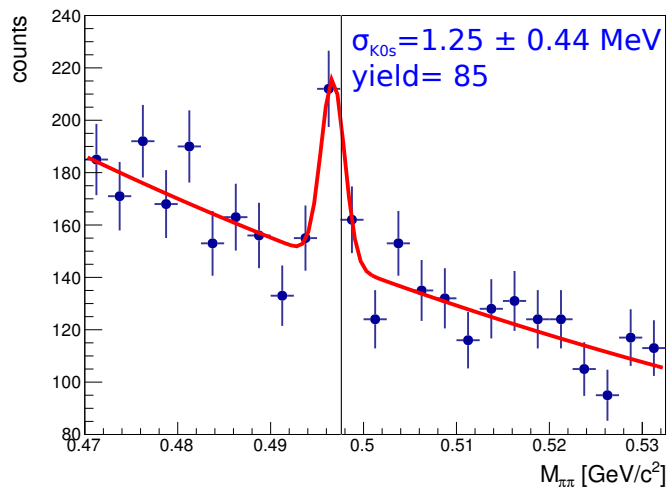
Figure 31: The reconstructed signal of K_s^0 particle. The black line corresponds to the K_s^0 mass taken from Ref. [33].

---

[4]Quark content: $\frac{d\bar{s} + s\bar{d}}{\sqrt{2}}$, mass: 497.611 ± 0.013 MeV, lifetime: $(0.8954 \pm 0.0004) \cdot 10^{-10}$ s [33]

From the data analysis it was observed, that the whole statistics can be divided into two samples:

- sample 1 (runs: 27256 - 27355) – with poor quality of K$_s^0$ signal,
- sample 2 (runs: 27384 - 27452) – with good quality of K$_s^0$ signal.

For data from sample 1 the signal can be visible only for the collisions which were taken at the end of this sample data taking. The comparison of results from both samples is presented in Figure 32. One can observe that the signals from different samples are not centered at the same mass. This shift is caused by the lack of final calibration of the data. It was found that between the registration of the data from both samples, there was a ten-hours break in the data taking. From this fact, one may conclude that something was changing in time during the data taking and was not corrected yet. This is why for the final analysis of D^0 signal only collisions from the second sample were used (about 140k events).
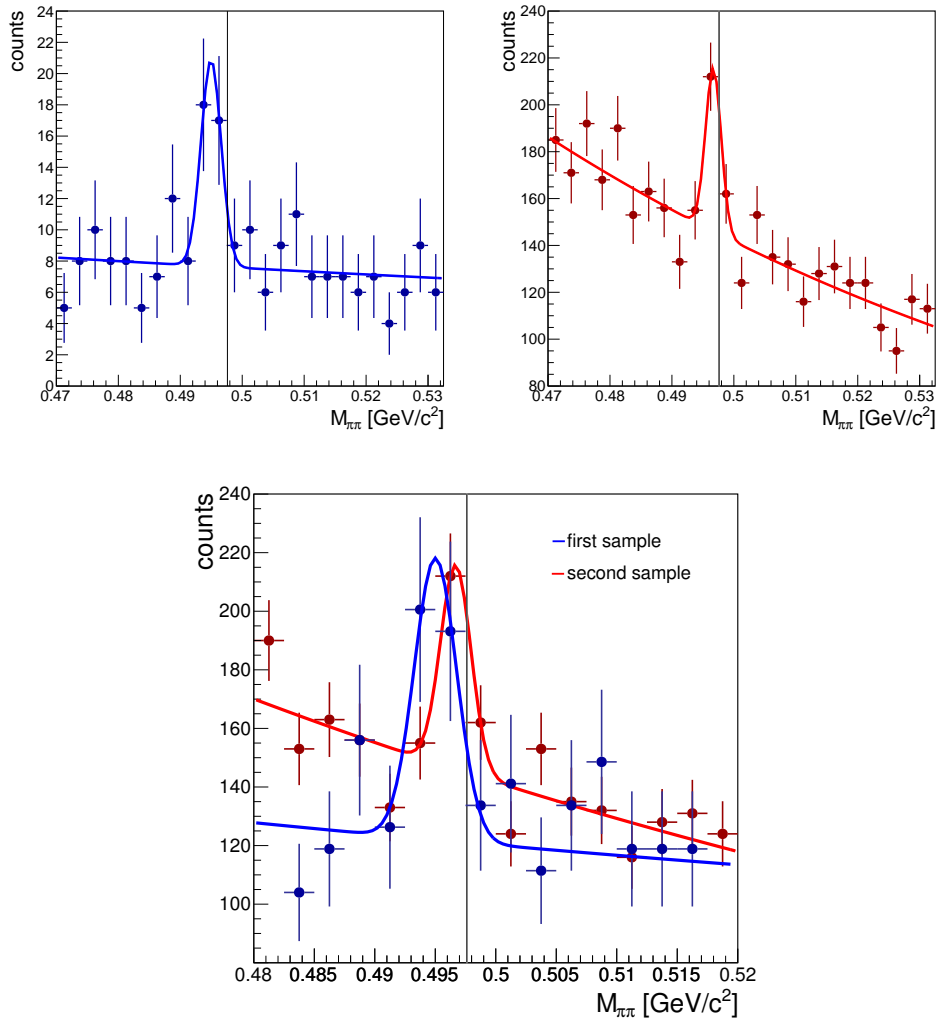
Figure 32: *Top Left*: K$_s^0$ signal obtained from first sample. *Top Right*: K$_s^0$ signal obtained from second sample. *Bottom*: The comparison of K$_s^0$ signal obtained from different samples of data. Data from first sample were scaled by eye. The black line corresponds to the K$_s^0$ mass taken from Ref. [33].

5.2   D^0 signal

The idea of D^0 measurement is described in Section 3.3. The analysis was performed using the Pb+Pb data at 150A GeV/c registered in December 2016, reconstructed using the algorithms discussed in Section 4. In order to reduce the background the track cuts described in Section 5.2.1 were applied. The final result is presented in Section 5.2.2.

5.2.1   Track cuts

The cut values were taken from Ref. [40]. These cuts are based on the simulation and are chosen to maximise the signal to noise ratio (SNR) for reconstructed D^0 peak. The values are presented in Figure 33 by the dashed vertical lines, together with the distributions of the variables for which the cuts were applied:

- p_T – transverse momentum – the momentum of daughter particle in the plane perpendicular to the beam axis,
- d – daughter particle impact parameter – the distance between the track and primary vertex,
- V_z – longitudinal position of the track pair vertex relative to primary vertex,
- d_p – mother particle impact parameter.

For experimental data the procedure of choosing the cut values is not finished yet. The corresponding distributions for experimental data are shown in Figure 34. Comparing the plots to the distributions presented in Figure 33, one may see that most of the primary tracks were removed from the analysis by the reconstruction algorithm (see Section 4). There are less tracks with small values of particle impact parameter (d). Also the peak in V_z distribution, which comes from primary tracks is significantly smaller. Based on presented plots, different cut values close to the values from simulation were tested and final cuts were selected as follows:

- transverse momentum: $p_T > 0.42$ GeV/c,
- track impact parameter: $d > 42$ μm,
- longitudinal position of the secondary vertex (reconstructed from track pair) relative to primary vertex: $V_z > 450$ μm,
- parent particle impact parameter: $d_p < 400$ μm.
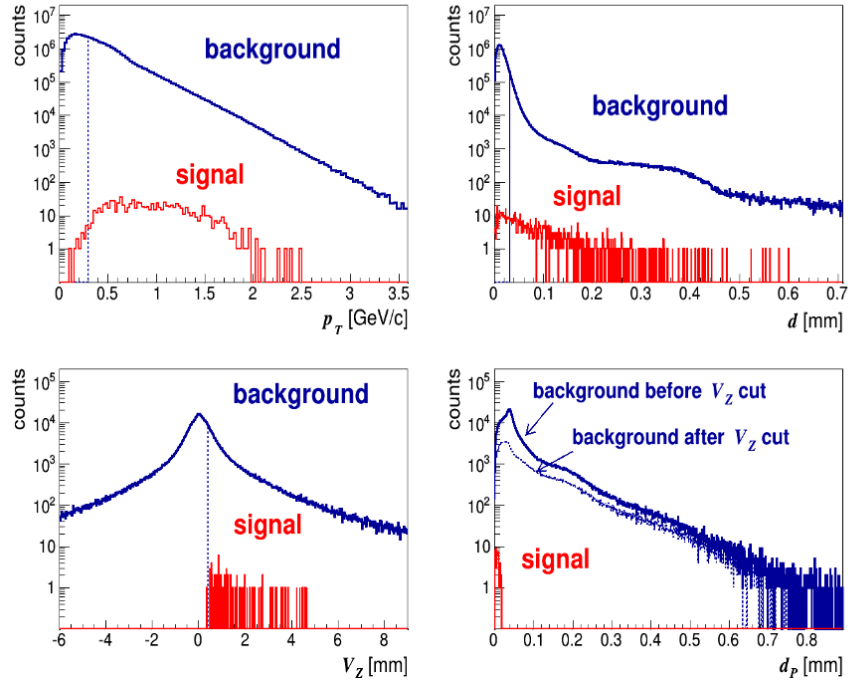
simulation

Figure 33: The distribution of the cuts variables from the simulation (AMPT model, Pb+Pb at 150*A* GeV/*c*) for D^0+$\overline{\text{D}^0}$ signal (red) and background (blue). The background distributions were obtained using all the tracks (primary and secondary). Figure from Ref. [40].
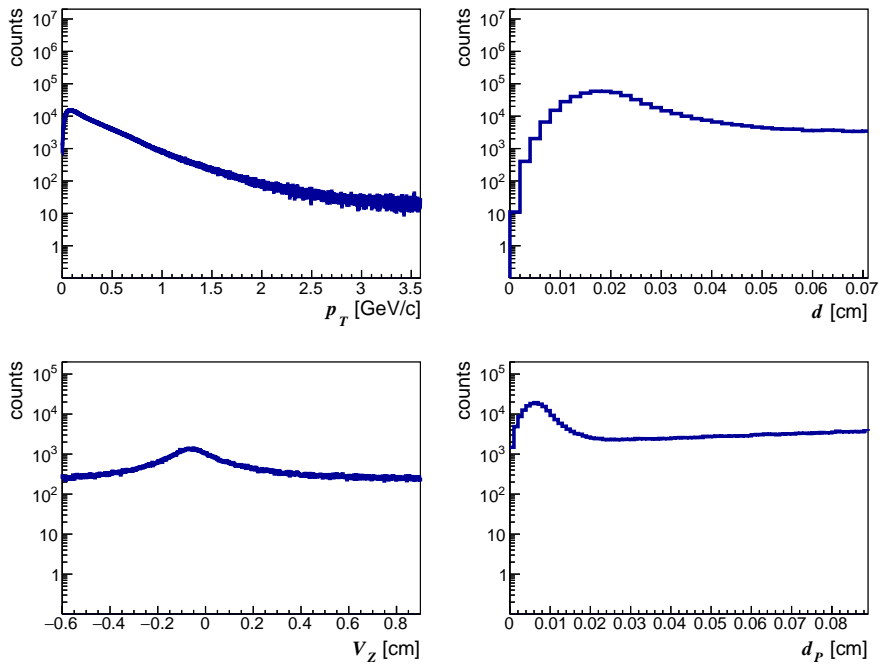
Figure 34: The distribution of the cuts variables from the reconstructed data.

5.2.2 Invariant mass distributions

The secondary tracks were reconstructed using the algorithms presented in Section 4. The track candidates which passed the cuts described in Section 5.2.1 were grouped into pairs. Then, for each pair the invariant mass was calculated assuming that the first particle is pion and the second kaon and vice versa. The particle identification of pions and kaons is planned to be done in the future. The obtained invariant mass distribution is presented in Figure 35. One may observe the clearly visible signal from D^0 and $\overline{D^0}$ decays. This important result confirms that NA61/SHINE is able to perform the direct measurement of open charm hadrons what is the main purpose of new physics programme of the experiment (see Section 3.2).

σ_{D0}=14.6 ± 3.2 MeV
yield = 62 ± 19
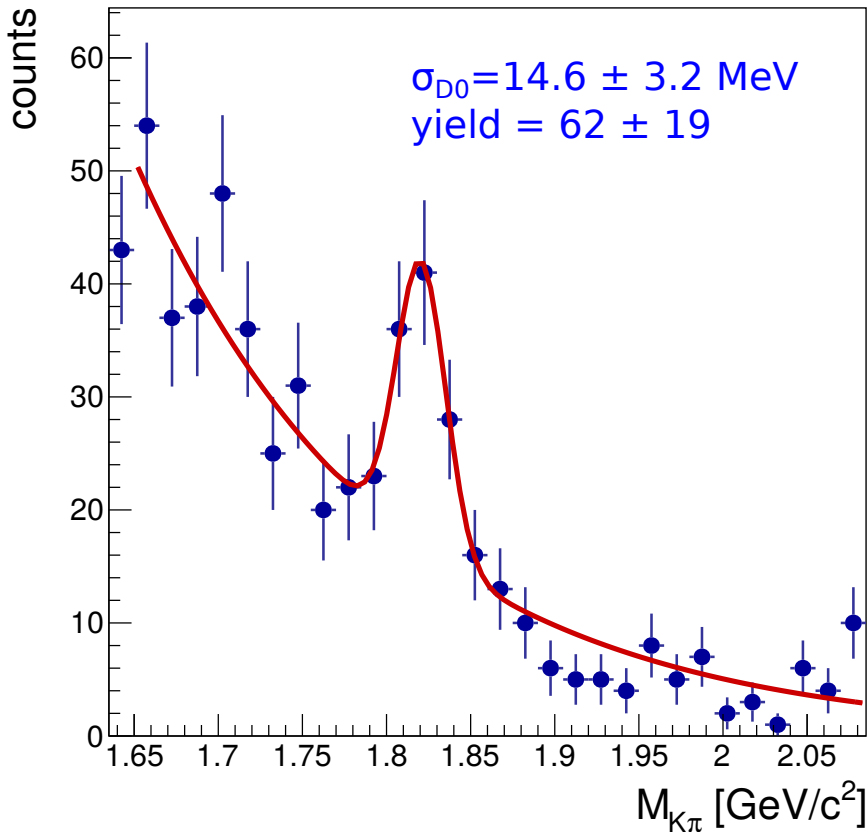
Figure 35: The invariant mass distribution of reconstructed secondary tracks assuming pion and kaon mass.

5.2.3 Comparison with different method

In the NA61/SHINE reconstruction software, there were implemented two methods of track matching between tracks reconstructed using VD and tracks reconstructed with other NA61/SHINE subdetectors; the track matching via extrapolation and via interpolation (implemented as a part of this

thesis, see Section 4.2). In the first method, the VD and TPC tracks were extrapolated to the common plane (VTPC-1 front surface) and the matching tracks were found [40]. Using this method also D^0 and $\overline{D^0}$ signal was observed. The comparison of the final signal obtained from both methods is presented in Figure 36. Comparing these methods, one may conclude that the interpolation method not only confirmed the obtained D^0 and $\overline{D^0}$ signal, but also improved the signal resolution by a factor of about 3.
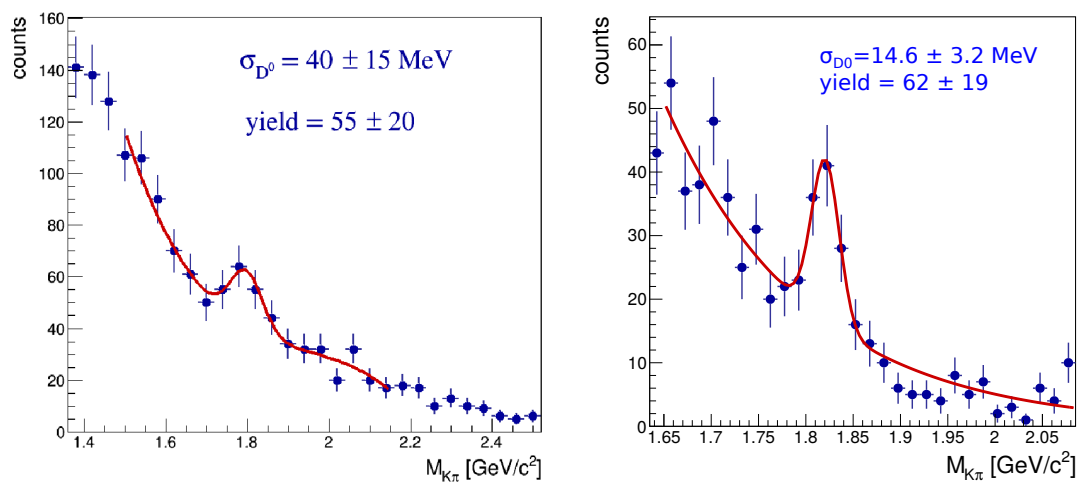
Figure 36: The invariant mass distribution of reconstructed secondary tracks assuming pion and kaon mass obtained from track matching via extrapolation [40] (*Left*) and via interpolation (*Right*).

6. Conclusions

This thesis has a significant input to the feasibility studies of new physics programme of the NA61/SHINE experiment. The programme is motivated by three main questions:

- What is the mechanism of open charm production?
- How does the onset of deconfinement impact open charm production?
- How does the formation of quark-gluon plasma impact J/ψ production?

In order to answer these questions, the knowledge of mean multiplicity of charm quark pairs $\langle c\bar{c} \rangle$ produced in a full phase space in heavy-ion collisions is needed. The measurement of the most popular charm mesons (D^0, $\overline{D^0}$, D^+, D^-) is enough to estimate the mean multiplicity of charm quark pairs. However, due to very short lifetime of these mesons, their measurement requires a micro vertex detector. In December 2016, the NA61/SHINE spectrometer was upgraded by a Small-Acceptance version of Vertex Detector and first pilot data for Pb+Pb collisions at 150A GeV/c were registered.

The first part of the work described in this thesis was to implement two algorithms used in data reconstruction. The first was the algorithm of the silicon sensors alignment. For this purpose the data taken without magnetic field were used. The geometry corrections were found by the minimisation of the distances between fitted track and collected clusters. The final results improved the clusters spatial resolution up to 20%. The second algorithm was the track matching between data reconstructed with SAVD and data from other subdetectors. The algorithm of matching via interpolation was used. At first, tracks are refitted to VD primary vertex (for primary tracks) or VD clusters from defined station (for secondary tracks) and then interpolated to other VD stations and the matching clusters are collected. Finally, the whole track is refitted using Kalman Filter.

After the data reconstruction, the analysis of K^0_s signal was performed to test the implemented algorithms. The signal was successfully observed. The analysis also showed the problem with data calibration, thus only the second half of collected statistics, which gave better results, was used for the final analysis.

The main aim of this work was to observe the first indication of D^0 and $\overline{D^0}$ signal in collisions of nuclei at the SPS energies. The proper analysis was performed and the distribution of invariant mass of pairs of reconstructed secondary tracks was calculated. The final result shows the clearly visible signal of D^0 and $\overline{D^0}$ decays. It is the first direct measurement of open charm hadrons in heavy-ion collisions at the SPS energies. However, the statistics is not enough to make some first conclusions on the charm production cross-section. The performed test measurement confirms, that using the new Vertex Detector, the NA61/SHINE experiment is able to reconstruct the signal from open charm hadrons decays and thus to perform high statistics studies on open charm production in heavy-ion collisions. The implemented algorithms and data analysis software will be also used for high statistics data which will be collected in the future.

Bibliography

[1] S. Weinberg, "*The Making of the standard model*", *Eur. Phys. J.*, vol. C34, pp. 5–13, 2004. arXiv:hep-ph/0401010 [hep-ph]. 13

[2] T. Czopowicz, "*Transverse momentum fluctuations in proton-proton and beryllium-beryllium interactions at the SPS energies*". PhD thesis, Warsaw University of Technology, 2018. 14, 53

[3] "Contemporary Physics Education Project". http://www.cpepweb.org/, Accessed: 20.05.2018. 15, 53

[4] "Lattice QCD, the numerical approach to the strong force". https://webific.ific.uv.es/web/en/content/lattice-qcd-numerical-approach-strong-force, Accessed: 20.05.2018. 15, 53

[5] "K. Grebieszkow. *Heavy Ion Physics lectures at Warsaw University of Technology*". http://www.if.pw.edu.pl/~kperl/HIP/hip.html, Accessed: 9.05.2018. 16, 53

[6] J. Rafelski and B. Muller, "*Strangeness Production in the Quark - Gluon Plasma*", *Phys. Rev. Lett.*, vol. 48, p. 1066, 1982. 17

[7] J. D. Bjorken, "*Energy Loss of Energetic Partons in Quark - Gluon Plasma: Possible Extinction of High p(t) Jets in Hadron - Hadron Collisions*". Technical Report FERMILAB-PUB-82-59-THY, FERMILAB, Batavia, IL, 1982. 17

[8] T. Matsui and H. Satz, "*J/ψ Suppression by Quark-Gluon Plasma Formation*", *Phys. Lett.*, vol. B178, pp. 416–422, 1986. 17, 23, 24

[9] U. W. Heinz, "*From SPS to RHIC: Maurice and the CERN heavy-ion programme*", *Phys. Scripta*, vol. 78, p. 028005, 2008. arXiv:0805.4572 [nucl-th]. 17

[10] L. Adamczyk *et al.* [STAR], "*Centrality dependence of identified particle elliptic flow in relativistic heavy ion collisions at $\sqrt{s_{NN}}$=7.7–62.4 GeV*", *Phys. Rev.*, vol. C93, no. 1, p. 014907, 2016. arXiv:1509.08397 [nucl-ex]. 17

[11] "NA49 library of images". 18, 53

[12] N. Abgrall *et al.* [NA61/SHINE], "*NA61/SHINE facility at the CERN SPS: beams and detector system*", *J. Inst.*, vol. 9, p. P06005, 2014. arXiv:1401.4699 [physics.ins-det]. 19

[13] "NA61/SHINE website". http://shine.web.cern.ch/, Accessed: 17.06.2018. 19

[14] "NA49 website". http://na49info.web.cern.ch/na49info/, Accessed: 17.06.2018. 19

[15] "NA61/SHINE library of images". 19, 20, 27, 33, 53, 54

[16] Z. Fodor and S. Katz, "*Critical point of QCD at finite T and μ, lattice results for physical quark masses*", *J. High Energy Phys.*, vol. 0404, p. 050, 2004. arXiv:hep-lat/0402006 [hep-lat]. 20

[17] A. P. Kostyuk, M. I. Gorenstein, H. Stoecker, and W. Greiner, "*Statistical coalescence model analysis of J/ψ production in Pb + Pb collisions at 158 A GeV*", *Phys. Lett.*, vol. B531, pp. 195–202, 2002. arXiv:hep-ph/0110269 [hep-ph]. 21, 53

[18] M. Gaździcki and M. I. Gorenstein, "*On the early stage of nucleus-nucleus collisions*", *Acta Phys. Polon.*, vol. B30, p. 2705, 1999. arXiv:hep-ph/9803462 [hep-ph]. 21, 53

[19] O. Linnyk, E. L. Bratkovskaya, and W. Cassing, "*Open and hidden charm in proton-nucleus and heavy-ion collisions*", *Int. J. Mod. Phys.*, vol. E17, pp. 1367–1439, 2008. arXiv:0808.1504 [nucl-th]. 21, 25, 53

[20] T. Song, private communication. 21, 25, 53

[21] R. V. Gavai, S. Gupta, P. L. McGaughey, E. Quack, P. V. Ruuskanen, R. Vogt, and X.-N. Wang, "*Heavy quark production in pp collisions*", *Int. J. Mod. Phys.*, vol. A10, pp. 2999–3042, 1995. arXiv:hep-ph/9411438 [hep-ph]. 21, 53

[22] P. Braun-Munzinger and J. Stachel, "*(Non)thermal aspects of charmonium production and a new look at J/ψ suppression*", *Phys. Lett.*, vol. B490, pp. 196–202, 2000. arXiv:nucl-th/0007059 [nucl-th]. 21, 53

[23] P. Levai, T. S. Biro, P. Csizmadia, T. Csorgo, and J. Zimanyi, "*The Production of charm mesons from quark matter at CERN SPS and RHIC*", *J. Phys.*, vol. G27, pp. 703–706, 2001. arXiv:nucl-th/0011023 [nucl-th]. 21, 53

[24] N. Antoniou *et al.* [NA49-future], "*Study of Hadron Production in Hadron-Nucleus and Nucleus-Nucleus Collisions at the CERN SPS*", Tech. Rep. SPSC-P-330. CERN-SPSC-2006-034, CERN, Geneva, Nov 2006. 21, 22, 23, 26, 28, 29, 30, 31, 53, 54

[25] R. V. Poberezhnyuk, M. Gaździcki, and M. I. Gorenstein, "*Open charm production in central Pb+Pb collisions at the CERN SPS: statistical model estimates*", *Acta Phys. Polon.*, vol. B48, p. 1461, 2017. arXiv:1708.04491 [nucl-th]. 22, 53

[26] R. V. Poberezhnyuk, private communication. 22, 53

[27] A. P. Kostyuk, M. I. Gorenstein, and W. Greiner, "*Heavy flavor enhancement as a signal of color deconfinement*", *Phys. Lett.*, vol. B519, pp. 207–211, 2001. arXiv:hep-ph/0103057 [hep-ph]. 22, 23, 53

[28] U. W. Heinz and M. Jacob, "*Evidence for a new state of matter: An Assessment of the results from the CERN lead beam program*", 2000. arXiv:nucl-th/0002042 [nucl-th]. 23

[29] H. Satz, "*Calibrating the In-Medium Behavior of Quarkonia*", *Adv. High Energy Phys.*, vol. 2013, p. 242918, 2013. 23, 53

[30] M. C. Abreu *et al.* [NA50, NA38], "*Dimuon and charm production in nucleus-nucleus collisions at the CERN SPS*", *Eur. Phys. J.*, vol. C14, pp. 443–455, 2000. 24

[31] M. C. Abreu *et al.* [NA50], "*Evidence for deconfinement of quarks and gluons from the J/ψ suppression pattern measured in Pb + Pb collisions at the CERN SPS*", *Phys. Lett.*, vol. B477, pp. 28–36, 2000. 24, 53

[32] R. Arnaldi *et al.* [NA60], "*J/ψ production in indium-indium collisions at 158-GeV/nucleon*", *Phys. Rev. Lett.*, vol. 99, p. 132302, 2007. 24

[33] C. Patrignani *et al.* [Particle Data Group], "The Review of Particle Physics (2017)". http://pdg.lbl.gov/, Accessed: 18.06.2018. 26, 40, 41, 55

[34] "MIMOSA26 User Manual". http://www.iphc.cnrs.fr/IMG/pdf/M26_UserManual_light.pdf, Accessed: 17.06.2018. 28

[35] Z.-W. Lin *et al.*, "*A Multi-phase transport model for relativistic heavy ion collisions*", *Phys. Rev.*, vol. C72, p. 064901, 2005. 28

[36] A. Aduszkiewicz *et al.* [NA61/SHINE], "*Beam momentum scan with Pb+Pb collisions*", Tech. Rep. CERN-SPSC-2015-038. SPSC-P-330-ADD-8, CERN, Geneva, Oct 2015. 29, 31, 54

[37] M. Mager [ALICE], "*ALPIDE, the Monolithic Active Pixel Sensor for the ALICE ITS upgrade*", *Nucl. Instrum. Meth.*, vol. A824, pp. 434–438, 2016. 30

[38] F. James and M. Winkler, "MINUIT User's Guide". http://seal.web.cern.ch/seal/documents/minuit/mnusersguide.pdf, 2004. 33

[39] R. Fruhwirth, "*Application of Kalman filtering to track and vertex fitting*", *Nucl. Instrum. Meth.*, vol. A262, pp. 444–450, 1987. 36

[40] A. Aduszkiewicz *et al.* [NA61/SHINE], "*Report from the NA61/SHINE experiment at the CERN SPS*", Tech. Rep. CERN-SPSC-2017-038. SPSC-SR-221, CERN, Geneva, Oct 2017. 42, 43, 45, 55

List of Figures